LAGRANGIAN TRANSPORT CALCIJLATIONS USING UARS DATA. PART 1: PASSIVE TRACERS

G. L. Manney[1], W. A. Lahoz[2], R. S. Harwood[3], R. W. Zurek[1],
J. B. Kumer[4], J. L. Mergenthaler[4], A. E. Roche[4], A. O'Neill[2],
R. Swinbank[5], J. W. Waters[1]

[1] Jet Propulsion Laboratory/California Institute of Technology
[2] Centre for Global Atmospheric Modelling, Reading UK
[3] Edinburgh University, Edinburgh UK
[4] Lockheed Palo Alto Research Laboratory
[5] Meteorological Office, Bracknell UK

Submitted to
Journal of the Atmospheric Sciences,
UARS Special Issue

Abstract

The transport of passive tracers observed by UARS has been simulated using computed trajectories of thousands of air parcels initialized on a three-dimensional stratospheric grid. These trajectories are calculated in isentropic coordinates using horizontal winds provided by the United Kingdom Meteorological Office data assimilation system and vertical (cross-i sentropic) velocities computed using a fast radiation code. The conservative evolution of trace constituent fields is estimated by assigning to each parcel the observed mixing ratio of the long-lived trace gases N_2O and CH_4 observed by CLAES and H_20 observed by MLS on the date of initialization. Both northern and southern hemisphere early and late winters are examined. Comparisons with observations interpolated to parcel positions show that large-scale characteristics of the calculated fields agree very well with observations, especially inside the polar vortex and during the late winter periods. Calculated fields show occurrences of very narrow tongues of material, which are at the limit of resolution of the UARS data, being drawn off the edge of the vortex into low latitudes; in some cases there is observational evidence of these features. Synoptic maps gridded from trajectory calculations in late winter reproduce all major features of the observations, including large tongues of material drawn from low latitudes into the polar regions during Feb and Mar 1993. Rough estimates are obtained for diabatic descent rates in the lower stratosphere. The overall agreement between the calculated and observed tracer fields supports the utility of these calculations in diagnosing trace species transport.

1. Introduction

Observations of passive tracers are invaluable in diagnosing air motions. Nitrous oxide (N_2O) measured by aircraft has been used to locate and describe the polar vortex and to estimate vertical velocities (Podolske et al. 1989, Loewenstein et al. 1990, Schoeberl et al. 1989, 1992, Strahan et al. 1994; and references therein). Manney et al. (1994b) used N_2O measurements from the Cryogen Limb Array Etalon Spectrometer (CLAES) on the Upper Atmosphere Research Satellite (UARS) to describe three-dimensional air motions during stratospheric warmings in February and March 1993; Lahoz et al. (1993) used CLAES N_2O and Microwave Limb Sounder (MLS) H_2O to examine vortex processes in the NH mid-stratosphere, and Harwood et al. (1993) used MLS H_2O data to describe transport during spring in the SH. Manney et al. (1994c) used N_2O measurements in comparison with MLS ozone measurements to qualitatively separate chemical and dynamical effects in the NH lower stratosphere.

Trajectory calculations provide another means of investigating air motions. Isentropic trajectory calculations (Bowman 1993, Chen et al. 1994, Chen 1994, Dahlberg and Bowman 1994) using winds derived from data have been used to study the degree of separation and mixing between polar vortex and mid-latitude air during winter in the lower stratosphere of both hemispheres. Pierce and Fairlie (1993) used winds from a general circulation model to examine mixing at the vortex edge in the Arctic winter. Fisher et al. (1993) used three-dimensional winds from a mechanistic model of the stratosphere and mesosphere to describe the general features of large scale air motion through the course of a SH winter. Manney et al. (1994a) used horizontal winds from the United Kingdom Meteorological Office (UKMO) data assimilation, system, and vertical velocities from a middle atmosphere radiation code to examine three-dimensional air motions and the mixing of polar and mid-latitude air for recent winters in both NH and SH.

Recent studies combine trajectory calculations and measurements of passive tracers to gain further insights into stratospheric air motions. Pierce et al. (1 994) initialize clusters of trajectories at the sunrise/sunset measurement locations of the UARS Halogen Occultation Experiment (HALOE), and assign to them the mixing ratio of trace species measured there by HALOE, These parcels are then advected forward in time on an isentropic surface using UKMO horizontal winds to "fill in" the relatively sparse coverage provided by UARS solar occultation measurements, and predict fields where HALOE did not measure. Morris et al. (1994) applied a similar technique to CLAES, HALOE and MLS data, by adding parcels to isentropic trajectory calculations at measurement locations and times, using winds calculated from National Meteorological Center (NMC) data. In this case, the air motion predicted by the trajectory calculation is used to simulate a higher resolution field than can be retrieved directly from UARS observations. Both studies focus on using the available meteorological information to enhance the resolution and/or extend the coverage of measurements, in effect as a mapping technique. Furthermore, numerical calculations show that even the use of moderately coarse resolution wind fields to compute advection (whether Lagrangian or Eulerian) can still capture higher resolution features of trace species distributions (e.g., Hsu, 1980; Waugh et al. 1994),

Here we use three-dimensional calculations of air parcel motion throughout the stratosphere, and observations of passive tracers from the CLAES and MLS instruments cm UARS to examine and compare the transport of passive tracers, The approach is different than that taken in the above-mentioned studies in that we initialize a three-dimensional grid of parcels on a given day with tracer mixing ratios taken from gridded UARS fields having nearly global coverage on a daily basis, Those parcels are then advected in three-dimensions using UKMO horizontal wind fields and a radiation calculation to obtain vertical velocities. This is in effect, a kind of transport code. Comparison of these results with observed fields will aid in understanding the relative importance of

horizontal and vertical transport,

We examine four thirty-day periods. During December 1992 and February-March 1993 in the NH, and August 1992 in the SH, measurements of N_2O and methane (CH_4) from CLAES, and water vapor (H_2O) from MLS are available. During the latter half of June 1992, N_2O and CH_4 from CLAES are available on most days. A solar array drive anomaly in early June 1992 cause most instruments to be turned off, and MLS H_2O data are not continuously available during this period, Because N_2O has been widely used to describe air motions and is a tropospheric source gas with an extremely long stratospheric lifetime, thus providing an ideal dynamical tracer, we focus in more detail on comparisons using N_2O. The two late winter time periods are of particular interest since they are both times when ozone depletion that can be ascribed to chemical loss has been observed (Waters et al. 1993a,b, Manney et al.1993, Manney et al.1994c) in the lower stratosphere.

2. **Data and Analysis**

The trajectory calculations are initialized on a grid similar to that described by Manney et al (1994a), "but the previous hemispheric coverage of initial parcel positions has been extended in latitude to 20° in the hemisphere opposite to the one of interest, so that cross-equatorial flow does not result in a lack of parcels at low latitudes. Parcels are initialized on a 2^{O} latitude by 5^{O} longitude grid, and at 13 levels throughout the stratosphere: 420, 465, 520, 585, 655, 740, 840, 960, 1100, 1250, 1400," 1650, and 1850 K. Horizontal winds are from the United Kingdom Meteorological office (UKMO) data assimilation system (Swinbank and O'Neil] 1994) and vertical velocities from a recent version of the middle atmosphere radiation code MI DRAD, an earlier version of which is described by Shine (1987), Temperatures in the radiation code are from the UKMO data; the runs considered here are thirty days long, and restricted to times when MLS and CLAES were

observing the hemisphere of interest. MLS ozone is used in the heating rate calculation, except for June 1992, when MLS ozone measurements are not continuously available. Manney et al. (1994a) discuss the impact of using climatological versus MLS ozone. The trajectory code (Manney et al. 1994a) uses a standard fourth-order Runge-Kutta scheme. Winds and temperatures are interpolated linearly in time from the once daily values to the trajectory time step (1/2 hour). Heating rates are recalculated every 3 hours using interpolated temperatures, and are interpolated linearly to the trajectory time step between calculations. Further details are given by Manney et al. (1994a).

The Rossby-Ertel potential vorticity (PV) is also calculated from the UKMO data (Manney and Zurek 1993) and is compared with calculated and observed tracer fields: PV is scaled in "vorticity units" (Dunkerton and Delisi 1986, Manney and Zurek 1993) when examining vertical cross-sections; this gives a similar range of values for PV on isentropic surfaces throughout the stratosphere.

The CLAES instrument is described by Roche et al. (1993), The utility of CLAES N_2O and CH_4 data for scientific purposes is described by Kumer et al. (1993). The data are still in the validation process; this process has verified that the data used here (v0006) are suitable for studies of morphology and regional variation. The most recent UARS validation workshop resulted in typical precision and systematic error estimates for N_2O of (20 ppbv rms, 20%) and (10 ppbv rms, 20%) on the 46 and 4.6 hPa surfaces, respectively, and for CH_4 of (100 ppbv, 20%) and (50 ppbv, 20%). A NASA report describing the UARS validation exercise is to be issued. At lower altitudes, when N_2O (CH_4) mixing ratios exceed ≈210 ppbv (=1,35 ppmv), values are suspect due to large line-of-sight opacity and the associated lack of tangent point sensitivity (Kumer et al. 1993). Because the vertical gradients of N_2O are generally steeper than those of CH_4 for the time periods considered here, N_2O values tend to be reliable over a larger portion of the vertical range we are considering.

The MLS H_2O data have horizontal resolution of ≈400 km and vertical resolution of ≈4 km. The UARS MLS instrument is described by Barath et al. (1993), and the H_2O data by Lahoz et al. (1994, paper in preparation). Single profile precision and accuracy estimates for H_2O are (0.3 ppmv, 15%) at 4.6 hPa (Harwood et al. 1993, Lahoz et al. 1993, Lahoz et al. 1994, paper in preparation). Between ≈20 hPa and 50 hPa, data quality is generally good only at low and middle latitudes. At high latitudes in winter, the data may have a substantial component from climatology at 50 hPa (Lahoz et al. 1994, paper in preparation), H_20 data are examined only from ≈20 hPa to ≈1 hPa here.

Both CLAES and MLS data have been mapped to a 4° latitude by 5^{O} longitude grid; this is consistent with the general meridional resolution of both instruments. CLAES data are gridded by linearly interpolating data for a 24 h period to a regular latitude-longitude grid; ascending and descending orbit tracks are treated separately and then averaged. MLS data are gridded using Fourier transform techniques that separate time and longitude variations (Elson and Froidevaux 1993). All data are interpolated to isentropic (θ) surfaces using UKMO temperatures.

Air parcels are initialized on the grid described above, on 15 Jun 1992 and 18 Aug 1992 in the SH, and 3 Dec 1992 and 14 Feb 1993 in the NH the trajectory code was run for 20 days for the June 1992 case, and 30 days for each of the other cases. The starting dates are chosen a few days after the beginning 'of the north or south-looking period, when CLAES data become available for the full day. The parcel's tracer mixing ratios are initialized by linearly interpolating the gridded UARS CLAES or MLS data described above to the 2(' latitude by 5° longitude initial parcel grid.

The evolution of the tracer fields is subsequently predicted by assigning the initial concentration to the locations of each parcel at later times, as determined by the forward trajectory calculations. Since these predicted parcel locations will not in general coincide with the points of the observational grid, the predicted fields are compared with observations by interpolating the observed fields to the parcel positions, or by gridding the

predicted fields at $4^{O} \times 5^{O}$. interpolation of data to predicted parcel positions is straightforward linear interpolation. A number of methods have been tried for gridding the parcel fields. For the fields shown here, the parcels were grouped in potential temperature bins centered around the initial levels listed above, according to their calculated θ. In each of these bins, the tracer mixing ratios and potential temperatures of the parcels are gridded by binning into 4^{O} latitude by 5° longitude boxes, with an average of the values for parcels in that box, weighted by distance from the center of the box, assigned to each box. Boxes with no parcels are then filled in by linear interpolation, unless many contiguous boxes are missing, in which case those boxes are simply treated as missing data in further analyses, In general, all of the gridding methods tried produced similar fields, especially in their large scale features. Since no new parcels are added during these simulations, by the end of the runs, many areas in approximately the top four levels are not covered.

3. Analyses at Parcel Positions

Manney et al. (1994a) show in some detai the amount and patterns of descent experienced by air parcels during the periods considered here. In general, the strongest descent in the middle and upper stratosphere is in the center of the vortex, with a secondary maximum in the NH along the vortex edge in the region between the vortex and anticyclone when wave activity is strong. In the. lower stratosphere, except in early winter in the NH, strongest descent is at the edge of the polar vortex,

Figure 1 shows predicted fields of N_2O on day (), 8,16 and 24 of each of the runs, compared with observed CLAES values cm those days that have been interpolated to the parcel positions, Since N_20 typically decreases with height, descent produces lower N_20 mixing ratios at a given level. Fields are shown for parcels initialized at 655 K in early winter, and at 840, 655 and 465 K in late winter. In all cases, the large-scale

features of the observed fields, particularly the rotation, displacement and elongation of the polar vortex are well reproduced by the predicted fields. Throughout the run started 14 February 1993, tongues of high N_2O air can be seen being drawn up around the polar vortex in both the observations and the trajectory calculations. The positions of these features in data and calculations correspond very well. In some instances very narrow features are seen in the trajectory calculations, for example, a narrow line of very high N_2O at 840 K over the southern United States on day 24 (1() Mar) of the simulation, and narrow filaments of low N_2O apparently drawn off the edge of the vortex at 655 K apparent on each of the days shown. These features are not well resolved in the observations, but some do have counterparts, for instance the line of high N_20 over the southern United States at 840 K, and the narrow tail of low N_20 drawn off the vortex at 655 K on the same day. A similar correspondence can be seen in some features of the fields for the run started18 Aug 1992 in the SH, for example, a narrow tongue of high N_20 that has been drawn up around the edge of the vortex on day 24(11 Sep).

In Feb/Mar 1993, the regions of high N_2O that are drawn up from low latitudes are generally somewhat larger and contain higher values in the trajectory calculations than in the data. This suggests the possibility that the winds in this region might be too strong, leading to more poleward transport than is observed; or the diabatic descent calculated by the radiation code used could be too weak in these regions. However, lower values could also be obtained in the observations by washing out strong gradients that cannot be resolved in the measurements.

The figures at 465 K in late winter show a good correspondence, in shape, position and evolution of the polar vortex, indicated by the region of low N_20, Outside this region, N_2O mixing ratios are generally higher than the maximum values in which we have confidence

By the end of the trajectory runs, a large degree of mixing is seen of parcels with high and low mixing ratios in mid-latitudes. This is mainly due to accumulated errors in

the positions of individual parcels over the course of the run (Morris et al. 1994), and in some cases to the inability of the relatively low horizontal resolution UARS data to resolve sharp gradients. In the early winter cases, distinct mid-latitude features have been washed out by the end of the runs,

To summarize average characteristics of the comparisons, we examined the average of observed tracer values interpolated to parcel positions for various ensembles of parcels. Figure 2 shows the average, maximum and minimum mixing ratios of parcels that were initialized on a given level, and whose scaled PV values indicated that they were within the polar vortex, as defined by the 1.4 x 10-4 s-1 scaled PV contour. CH_4 and H_20 are shown in addition to N_2O where available. Manney et al. (1994a) show that, for the periods considered here, nearly all the parcels remain within the vortex, except during the last ≈10 days of the run started 14 Feb 1993, when the vortex shrinks and weakens in the middle and upper stratosphere due to strong stratospheric warmings (Manney et al. 1994b). At that time many parcels are drawn out into low latitudes, as well as moving to lower PV values due to radiative (and other non-conservative) effects. If a parcel exactly followed atmospheric motions, the mixing ratio of a passive tracer would remain constant at its location, and no change would be seen in minimum, maximum, or average values. Thus, trends shown in Fig. 2 represent nonconservative processes, possibly due to a combination of 1) errors in the trajectory calculations; 2) lack of resolution or coverage, or errors in the observations; or 3) "truly nonconservative physical processes. Since the tracers considered here are long-lived photochemically, the last of these possibilities should not be significant, except for state changes in H_20.

For most of the time periods shown here, these averages show little trend, suggesting that the combination of vertical and horizontal tranport predicted by the trajectory model for the vortex region is reasonable. Within the vortex, it is expected that changes in tracer mixing ratios result primarily from vertical motions, since horizontal mixing across the vortex edge is limited (e.g., Schoeberl et al 1992, Manney et al. 1994a, and

references therein). This is less likely to be the case during times of particularly strong wave activity. During the late winter periods shown, low N_2O and CH_4 have descended in the vortex from the mesosphere to the mid-stratosphere (Kumer et al.1993, Fisher et al. 1993, Tuck et al. 1993, Manney et al. 1994a). At this time, vertical gradients of N_2O and CH_4 in the vortex are not very strong above ≈840 K, so at this level, the test is not as sensitive. Similar patterns are seen, however, at 655 K, where vertical gradients are stronger in the vortex, In the last ≈10 days of the run started on 14 Feb 1993, CLAES N_2O and CH_4 values increase, while MLS H_2O values decrease. This behavior begins at the onset of a strong stratospheric warming, from which the vortex never recovers to any large degree (Manney et al, 1994b); at this time, the area enclosed by the region of strong PV gradients decreases, and the strong gradients move to higher PV values (Manney et al. 1994a, this issue). Thus, more horizontal mixing is expected at this time at PV values included in this average. The increase in observed values could indicate either that the trajectory model predicts less transport of low latitude air into the polar vortex region (or more transport of vortex air toward lower latitudes), or that the radiation calculation predicts diabatic descent during the warming that is stronger than observed in the polar regions. MLS H_2O values decrease at parcel positions in Aug 1992, for parcels started at 840 K. MLS H_2O observations at this time show maximum mixing ratios in the polar regions near ≈1100 K. However, these maximum values lack obvious continuity from day to day, and do not appear to descend to lower levels. These observations have yet to be explained, but do not appear consistent with expectations of the behavior of passive tracers.

Figure 3 shows times series of the average observed N_2O mixing ratios as in Fig. 2, but with the parcels started at a given level binned in narrow PV bands, for parcels initialized at 840 K; similar features are seen for parcels initialized at 655 K. in late winter, little trend is seen in any of the fields, except for the last ≈10 days of the 14 Feb NH run in the vortex region, as discussed above. At low PV values there is a small increasing trend

in early winter, reflecting the washing out of high N_2O regions that was seen in the trajectory runs during this period. The fact that this trend is small suggests that, although specific features are not well reproduced, the average characteristics are still similar to observations. The 465 K fields in late winter (not shown) also show little trend at any PV values, suggesting that the trajectory calculation does a good job of transporting N_2O.

4. Gridded Fields

Although the above analyses give some insight into where the trajectory calculation simulates the observations well, for more detailed analysis it is desirable to produce a gridded field on isentropic surfaces. Figure 4 gives an example of the effect of the gridding procedure on the fields, for a case that is particularly problematic. N_2O and potential temperature values on the last day of the 14 Feb 1993 NH run are shown at the parcel positions in the potential temperature bin surrounding the 840 K level (788-897 K); the 840 K field that results from interpolating in θ using the gridded versions of these is also shown. In the middle and upper stratosphere, because some parcels have descended into a bin below their original bin, parcels near the top (high θ) are found in close proximity to parcels near the bottom (low θ) of the same bin, which may lead to undue smoothing in the θ field that is used to interpolate the horizontally gridded tracer field to an isentropic surface. This problem becomes much less severe at lower levels where most of the parcels remain in the same bin throughout the run; in all the simulations shown here, for instance, the parcels that begin at 465 K all remain in the bin surrounding that level throughout the integration.

Figure 5 shows synoptic maps of N_2O from the trajectory calculation compared with observations at 655 K during the early winter time periods. Several PV contours in the region of strong PV gradients are shown on the plot of observed fields to indicate the position and extent of the polar vortex. Again, the agreement is seen to be very good

within the polar vortex. As was apparent when observations were interpolated to parcel positions, the trajectory calculation does not do a good job of reproducing regions of high N_2O in mid-latitudes in early winter. In fact, some of these regions outside the vortex are not particularly well correlated with PV; since the trajectory calculations use the same winds from which the PV is calculated, they would not reproduce such features. Figure 6 shows synoptic maps of MLS H_2O compared with those calculated from trajectories at 655 K for the run started 3 Dec 1992, Horizontal gradients of H_20 are very weak outside the edge of the vortex, but there appears to be a slightly better correlation between calculated and observed H_2O, to the extent that, for the first ≈20 days of the run, most of the higher H_20 values that are stripped off the vortex correspond to predicted regions of higher H_20. This suggests that some of the difference between calculated and observed N_20 in early winter may be due to inaccuracies in the observed N_20 fields. A large part of the difference, however, must still be attributed to errors accumulated in the trajectory calculations, which produce different effects on tracers with different spatial gradients.

As noted by Manney et al. (1994b), in Feb and Mar 1993 (late winter), N_2O appears to be very well correlated with PV throughout the regions where N_20 measurements are considered reliable. This is also the case for the predicted fields generated here. Figure 7 shows synoptic maps of N_20 for the NH and SH late winter periods at 840 and 465 K, At 840 K (and 655 K, which is not shown), the calculated fields agree well with the observed fields throughout the simulations. At 840 K in the 14 Feb NH run, the blobs of high N_20 drawn in from low latitudes usually appear somewhat larger in the trajectory calculations. This is likely related to the much stronger gradients around these fields in the calculations. The UARS instruments cannot resolve gradients this sharp, if such gradients truly exist. Calculated tracer gradients may also be sharper than actual gradients, because no parameterization of small scale mixing is included in these calculations,

In the SH run starting 18 Aug 1992, at 655 K, minimum calculated N_2O values are slightly higher than he observed values, while at 840 K they are slightly lower. Since

diabatic descent is expected to be the main cause of trends in a tracer within the vortex, this would 'tend to suggest that the vertical distribution of diabatic cooling in the polar regions is somewhat different than that in the atmosphere, with slightly higher (lower) rates at 840 K (655 K). In the NH run from 14 Feb 1993, both 840 K and 655 K calculated minimum N_2O values at the end of the run are slightly lower than observed. This would suggest the possibility of slightly stronger descent in the model than in the atmosphere at these levels.

At 465 K, we restrict our attention to the vortex region, since N_2O (and CH_4) mixing ratios outside this region are higher than we have confidence in. Although the correspondence is not as striking as at higher levels, there is still a strong resemblance between the size and shape of the region of low N_2O and the vortex as defined by PV, and consequently, a strong correspondence between the observed and calculated low N_2O regions. In both the 14 Feb NH run and the 18 Aug SH run, minimum N_2O values at the end of the run appear nearly the same in observations and calculations, suggesting that the diabatic cooling rates used in the calculations are not significantly different from the atmospheric ones,

Figure 8 shows zonal mean fields as a function of latitude and θ from observations and trajectory calculations on day O and 24 (20 for Jun 1992) of each run, As might be expected from the above discussion, in early winter, the main-vortex/surf-zone structure (McIntyre and Palmer 1985) does not build up as strongly in the predicted fields as in observations. In particular, the sub-tropical region of strong N_20 gradients does not sharpen as much in the predicted fields. In the NH, the strengthening of the region of strong PV gradients along the edge of the polar vortex" is nearly as strong as in observations. Changes in the positions of N_20 contours suggest that calculated diabatic descent is somewhat too strong overall in the Dec 92 NH case, and somewhat too weak overall in the Jun 92 SH case.

In the late winter cases, changes in the zonal means are generally well reproduced, with only a slight weakening in the region of strong N_2O gradients in the sub-tropics. The vertical changes in the positions of contours are smaller here, but what changes there are suggest that, in the Feb 93 NH case, calculated descent rates are if anything, slightly stronger in the polar regions than in the atmosphere (deduced from the observed changes), In the SH, calculated descent rates appear somewhat too weak.

To examine in more detail differences in descent rates, we look at time series of vortex averaged tracers for the lower stratosphere (420 - 655 K) and middle stratosphere (655 - 1300 K) regions; Figure 9 shows these for N_2O. Except for the last ≈10 days of the run started 14 Feb 1993 in the NH, we expect descent to be the primary cause of changes in these averages. The plots for the middle stratosphere are somewhat difficult to compare, since, especially in late winter, the vertical gradients of N_2O are not particularly strong. Also, as mentioned above, above ≈1100 K, the trajectory fields have large gaps in the polar regions by the end of the runs, where parcels have descended below those levels. However, most of the major features in the observations are reproduced in the trajectory calculation below ≈900 K, including temporary increases in N_2O seen in the Dec 92 and Feb 93 runs, around 7, 15 and 24 Dee, and around 24 Feb and 10 Mar. These increases occur at times of particularly strong wave activity, and are probably due to large tongues of high N_2O being drawn up into the vicinity of the vortex from low latitudes. Since the region of strong PV gradients moves to higher PV values at this time (Manney et al. 1994a), some of these high values may be included in the average shown here. Overall trends suggest that, consistent with the previous figures, calculated descent rates are too strong for the Dec 92 NH run, and too weak for the Aug 92 SH run,

In the lower stratosphere we expect these area averages to be dominated even more strongly by descent, since wave activity is weaker, Rough estimates of descent rates in the lower stratosphere have been calculated from the information in these figures. In Dec 1992, the calculated N_2O evolution implies diabatic descent of ≈ 1.5 K/d (in potential

temperature, i e., $d\theta/dt$) at ≈550 K, while the observed evolution implies a rate of ≈ 1 K/d. in Jun 1992, the calculations imply a rate of ≈0.8 K/d and the observations ≈1.3 K/d at ≈550 K. This is the lowest level at which they can be estimated in early winter, since" below this, observed N_2O and CH_4 values are too high to be reliable.

in late winter, in Feb/Mar 1993, the calculated evolution implies a rate of= 1 K/d at ≈470 K, while observed evolution gives ≈0.6 K/d. In the SH in Aug/Sep 1992, the calculated value at this level is ≈0.2 K/d. The observed value is more difficult to estimate, as there appears to be a discontinuity around 1 September, with an abrupt downward shift of the contours after that time. Values calculated separately for the period before and after this yield rates of ≈0.2 --0.4 K/d; a calculation using just the endpoints of the time series would give ≈0.7 K/d.

Following the same procedure using CH_4 gives very similar results in each case. As expected, the estimates from the calculated fields are consistent with estimates by Manney et al. (1994a) computed directly from examination of air parcel positions, except during Aug/Sep 1992 in the SH. In that case the field gridded using the trajectory calculations suggests a descent rate approximately half that estimated directly from the parcel positions. This may indicate some irregularities in the observed CLAES fields used to initialize this run.

5. Summary

Trajectory calculations in which air parcels are initialized on a three-dimensional grid filling the stratosphere in one hemisphere are used to examine transport, by assigning to each parcel the observed mixing ratio of an atmospheric trace species on the initial day and then tracking the parcel locations on subsequent days. This technique is applied to passive tracer data, namely N_2O and CH_4 from CLAES and H_2O from MLS. Four 20 to 30 day time periods are examined, corresponding to periods when the two UARS

instruments were viewing high latitudes during early and late winter in the NH and SH.

Comparisons with observations by interpolating observed fields to parcel positions show that the average characteristics of the calculated fields agree well with observations, and especially well inside the polar vortex. Comparisons of individual parcel values show that, in early winter, the trajectory model tends to randomize the mixing ratios in mid-latitudes, with many parcels with high and low mixing ratios in close proximity. This may be due to accumulated errors in the parcel positions in regions where the winds are relatively weak, and thus errors in advection are likely to become large compared to the advection itself, It may also reflect the absence of small scale mixing in the trajectory calculations. The spatial resolution of the UARS data is not sufficiently great to test the predicted fields on this scale.

In late winter, the calculated and observed values at parcel positions agree well everywhere, and the trajectory model reproduces large tongues of high N_2O that are drawn from low latitudes around the vortex into the region of the anticyclone during Feb and Mar 1993. The predicted fields show a number of instances in the NH, and a few in the SH, where very narrow tongues of material are drawn off the edge of the vortex into low latitudes, The detection of such tongues by the low resolution satellite instruments would depend on the exact measurement locations (e.g., Morris et al. 1994) at that time, and in fact we show cases where there is some observational evidence of such features, and cases where there is not. Waugh et al. (1994) showed similar "filamentation" type behavior in very high resolution contour advection calculations for the Arctic winter stratosphere.

Comparisons have also been made between gridded fields from the trajectory calculations and from observations. Synoptic maps of predicted fields in late winter reproduce all major features of the observations. During the stratospheric warmings in Feb and Mar 1993 when large tongues of material are drawn from low latitudes into the polar regions, tracer gradients are considerably stronger in the calculations than the observations, This

is due mainly to two factors: 1) the low horizontal resolution of the satellite measurements smoothing the gradients in observed fields, and 2) the lack of any small scale mixing, except that caused artificially by the binning and interpolation to a grid, in the transport calculation,

Comparisons of calculated and observed zonal mean and vortex averaged fields give some insight into how calculated and observed descent rates compare in the lower stratosphere. Rough estimates indicate that in both of the NH cases, the radiation calculation used in the trajectory code predicts larger descent rates than are consistent with the tracer observations. In both of the SH cases, the calculation predicts smaller descent rates than the observations. In late winter 1992, the range of values suggests that in the SH, between 450-500 K in a vortex average, $d\theta/dt$ is not greater than ≈ 0.7 K/d and not less than ≈ 0.2 K/d. In the NH late winter in 1993, at the same level, calculations suggest that $d\theta/dt$ is between ≈ 0.6 and ≈ 1.0 K/d. These values are comparable to those given by Schoeberl et al. (1992) for late winter in the SH in 1987, and for mid-winter in the NH in 1989.

The overall agreement between the calculated and observed long-lived tracer fields indicates that trajectories calculated using the horizontal winds from the UKMO data assimilation system and computed diabatic vertical (cross-isentropic) velocities provide a reasonable approximation to conservative mass transport, at least at the middle and lower stratospheric levels, middle and polar latitudes, and wintertime periods examined here in detail, In addition to diagnosing atmospheric motions in a variety of stratospheric contexts, this trajectory approach can provide a baseline against which the evolving distributions of stratospheric trace gases can be examined for nonconservative effects, including the action of photochemistry on shorter-lived trace constituents such as ozone (Manney et al. 1994d).

Acknowledgments. We thanks our MLS and CLAES colleagues for their continued collaboration and support; L. S. Elson for providing mapped MLS data; T. Luu for data management; P. A. Newtnan for routines that were adapted to calculate PV. This research was sponsored by NASA's Upper Atmosphere Research Satellite Project and was performed at the Jet Propulsion Laboratory, California Institute of Technology under contract with the National Aeronautics and Space Administration.

References

Barath, F. T., M. C. Chavez, R. E. Cofield, D. A. Flower, M. A. Frerking, M. B. Gram, W. M. Harris, J. R. Holden, R. F. Jarnot, W. G. Kloezeman, G. J. Klose, G. K. Lau, M. S. Loo, B. J. Maddison, R. J. Mattauch, R. P. McKinney, G. E. Peckham, H. M. Pickett, G. Siebes, F. S. Soltis, R. A. Suttie, J. A. Tarsala, J. W. Waters, and W. J. Wilson, 1993: The Upper Atmosphere Research Satellite Microwave Limb Sounder instrument, *J. Geophys. Res.*, 98, 10,751-10,762.

Bowman, K, P., 1993: Large-scale isentropic mixing properties of the Antarctic polar vortex from analyzed winds, *J. Geophys. Res.*, 98, 23,013-23,027.

Chen, P., 1994: The permeability of the Antarctic vortex edge, *J. Geophys. Res.*, *submitted.*

Chen, P., J. R. Holton, A. O'Neil], and R. Swinbank, 1994: Quasi-horizontal transport and mixing in the Antarctic stratosphere, *J. Geophys. Res.*, submitted.

Dahlberg, S. P., and K. P. Bowman, 1994: Climatology of large-scale isentropic mixing in the Arctic winter stratosphere from analyzed winds, *J. Geophys. Res.*, submitted.

Dunkerton, T. J., and D. P. Delisi, 1986: Evolution of potential vorticity in the winter stratosphere of January-February, 1979. *J. Geophys. Res.*, **91, 1199-1208.**

Elson, L. S., and L. Froidevaux, 1993: The use of Fourier transforms for asynoptic mapping: Early results from the Upper Atmosphere research Satellite Microwave Limb Sounder, *J. Geophys. Res.*, **98,23,039-23,049**

Harwood, R. S., E. S. Carr, L. Froidevaux, R. F, Jarnot, W. A. Lahoz, C. L. Lau, G. E. Peckham, W. G. Read, P. D. Ricaud, R. A. Suttie, J. W. Waters, 1993: Springtime stratospheric water vapour in the Southern Hemisphere as measured by MLS, *Geophys. Res. Lett.*, 20, 1235-1238.

Hsu, C.-P. F., 1980: Air parcel motions during a numerically simulated sudden stratospheric warming, *J. Atmos. Sci., 37, 2768-2792.*

Kumer, J. B., J. L, Mergenthaler, and A. E. Roche, 1993: CLAES CH_4, N_2O, and CCL_2F_2 (F] 2) global data, *Geophys. Res. Lett.,* **20, 1239-1242,**

Lahoz, W. A., E. S. Carr, L. Froidevaux, R. S. Harwood, J. B. Kumer, J. L. Mergenthaler, G. E. Peckham, W. G. Read, P. D. Ricaud, A, E. Roche, J. W. Waters, 1993: Northern Hemisphere mid-stratospheric vortex processes diagnosed from H_2O, N_2O and potential vorticity, *Geophys. Res. Lett., 20,2671-2674.*

Loewenstein, M., J. R. Podolske, K. R. Chan, and S. E. Strahan, 1990: N_2O as a dynamical tracer in the Arctic vortex, *Geophys. Res. Lett., 17, 477-480.*

Manney, G. L., and R. W, Zurek, 1993: Interhemispheric comparison of the development of the stratospheric polar vortex during fall: A 3-dimensional perspective for 1991-1992. *Geophys. Res. Lett., 20, 1275-1278,*

Manney, G. L., L. Froidevaux, J. W. Waters, L. S. Elson, E, F, Fishbein, R. W. Zurek, R. S. Harwood, and W. A. Lahoz, 1993: The evolution of ozone observed by [JARS MLS in the 1992 late winter southern polar vortex. *Geophys. Res. Lett.,* 20, 1279-1282.

Manney, G. L., R. W. Zurek, A. O'Neil], and R. Swinbank, 1994a: On the motion of air" through the stratospheric polar vortex, *J. Atmos. Sci.,* submitted (this issue).

Manney, G. L., R. W. Zurek, A. O'Neil], R. Swinbank, J. B. Kumer, J. L. Mergenthaler, and A, E. Roche, 1994b: Stratospheric Warmings during February and March 1993. *Geophys. Res. Lett.,* in press.

Manney, G. L., L. Froidevaux, J. W. Waters, R. W. Zurek, W. G. Read, L. S. Elson, J. B. Kumer, J. L. Mergenthaler, A. E. Roche, A, O'Neil], R, S. Harwood, 1. MacKenzie, and R. Swinbank, 1994c: Chemical Depletion of Lower Stratospheric Ozone in the 1992-1993 Northern Winter Vortex, *Nature,* submitted.

Manney, G.L., L. Froidevaux, R. W. Zurek, J. W. Waters, A.O'Neill, and R. Swinbank, 1994d: Lagrangian transport calculations using UARS data. Part 11: Ozone, *J. Atmos. Sci.*, submitted (this issue),

McIntyre, M. E., and T. N. Palmer, 1984: The 'surf zone' in the stratosphere, *J. Atmos. Terr. Phys.*, *46,825-849.*

Morris, G. A., M. R. Schoeberl, L. Sparling, P. A. Newman, L. R. Lait, L. S. Elson, J. W. Waters, A. E. Roche, J. B. Kumer, and J. M. Russell, 111, 1994: Trajectory mapping of Upper Atmosphere Research Satellite (UARS) data, *J. Geophys. Res.*, submitted.

Pierce, R. B., and T. D. A. Fairlie, 1993: Chaotic advection in the stratosphere: Implications for the dispersal of chemically perturbed air from the polar vortex, *J. Geophys. Res.*, 98, 18,589-18,595.

Pierce, R. B., W. L. Grose, J. M. Russell III, and A. F. Tuck, 1994: evolution of Southern Hemisphere spring air masses observed by HALOE, *Geophys. Res. Lett.*, **21,** 213-216.

Plumb, R. A., D. W. Waugh, R. J. Atkinson, P. A. Newman, L R. Lait, M. R. Schoeberl, E. V. Browell, A. J. Simmons, and M. Loewenstein, 1994: Intrusions into the lower stratospheric Arctic vortex during the winter of 1991-1992, *J. Geophys. Res.*, 99, 1089-1105.

Podolske, J. R., M. Loewenstein, S. E. Strahan, and K. R. Chan, 1989: Stratospheric nitrous oxide distribution in the Southern Hemisphere, *J. Geophys. Res.*, **94,** 16,767-16,772.

Proffitt, M. H., K. K, Kelly, J. A. Powell, B, L. Gary, M. Loewenstein, J. R. Podolske, S. E. Strahan, and K. R, Chan, 1989: Evidence of diabatic cooling and poleward transport within and around the 1987 Antarctic ozone hole, *J. Geophys. Res.*, 94, 16,797-16,814.

Proffitt, M. H., J. J. Margitan, K. K. Kelly, M. Loewenstein, J. R. Podolske, and K. R. Chan, 1992: Ozone loss in the Arctic polar vortex inferred from high-altitude aircraft measurements, *Nature,* 347,31-36, 1992.

Roche, A. E., J, B. Kumer, J. L. Mergenthaler, G. A. Ely, W. G. Uplinger, J. F. Potter, T. C. James, and L. W. Sterritt, 1993: The Cryogenic Limb Arrary Etalon Spectrometer (CLAES) on UARS: experiment description and performance, *J. Geophys. Res.,* 98, 10,763-10,775.

Russell, J. M. 111, A. F. Tuck, L. F. Gordley, J. H. Park, S. R. Drayson, J. E. Harries, R. J. Cicerone, and P. J. Crutzen, 1993: HALOE Antarctic observations in the spring of 1991, *Geophys. Res. Lett.,* 20,719-722,

Schoeberl, M. R., L. R. Lait, P. A. Newman, R. L. Martin, M. H. Proffitt, D. L. Hartmann, M. Loewenstein, J. Podolske, S. E. Strahan, J. Anderson, K. R. Chan, and B. L. Gary, 1989: Reconstruction of the constituent distribution and trends in the Antarctic polar vortex from ER-2 flight observations, *J. Geophys. Res.,* 94, 16,815-16,846.

Schoeberl, M. R., L. R. Lait. P. A. Newman, and J. E. Rosenfield, 1992: The structure of the polar vortex. *J. Geophys. Res.,* 97,7859-7882.

Shine, K. P., 1987: The middle atmosphere in the absence of dynamic heat fluxes. *Quart. J. Roy. Meteor. Soc., 113,603-633.*

Strahan, S. E., J. E. Rosenfield, M. Loewenstein, J. R. Podolske, and A. Weaver, 1994: The evolution of the 1991-2 Arctic vortex and comparison with the GFDL ' SKY HI' general circulation model, *J. Geophys. Res.,* submitted,

Swinbank, R., and A. O'Neill, 1994: A Stratosphere-troposphere data assimilation system, *Mon. Wea. Rev.,* **122,686-702.**

Tuck, A, F., J. M. Russell 111, and J. E. Harries, 1993: Stratospheric Dryness: Antiphased desiccation over Micronesia and Antarctica, *Geophys. Res. Lett.,* **20, 1227-1230.**

Waugh, D. W., R. A. Plumb, R. J. Atkinson, M, R. Schoeberl, L, R. Lait, P. A. Newman, M. Loewenstein, D. W. Toohey, L. M, Avallone, C. R. Webster, and R. D. May, 1994: Transport out of the lower stratospheric Arctic vortex by Rossby wave breaking, *J. Geophys. Res.*, 99, 1071-1088.

Waters, J. W., L. Froidevaux, W. G. Read, G. L. Manney, L. S. Elson, D. A. Flower, R. F. Jarnot, and R. S. Harwood, 1 993a: Stratospheric ClO and O_3 from the Microwave Limb Sounder on the Upper Atmosphere Research Satellite, *Nature, 362, 597-602.*

Waters, J. W., L. Froidevaux, G. L. Manney, W. G. Read, and L. S. Elson, 1993b: MLS observations of lower stratospheric C1O and O_3 in the 1992 southern hemisphere winter, *Geophys. Res. Lett,* 20, 1219-1222.

Figure Captions

Figure 1. Predicted and observed N_2O (ppbv) on days (), 8,16, and 24 of each of the 4 runs considered here (early and late winter, NH and SH). Predicted values are the values at the parcel positions on the initial day, advected with the parcels. Observed values are interpolated to the parcel positions from the gridded UARS data on each day. Fields are shown for parcels started at 655 K in early winter, and at 840, 655, and 465 K in late winter. Most of the parcels shown are moving downwards during the runs.

Figure 2. Average (circles), minimum (triangles) and maximum (squares) observed mixing ratios (ppmv) of N_2O, CH_4, and H_20, for the ensemble of parcels that were initially inside (i.e., at higher PV than) the 1.4 x 10^{-4} s^{-1} scaled PV contour (-PV in the SH). Observed values are interpolated to parcel positions on each day, and the average, minimum and maximum of these values are shown. Values are shown for parcels started at 840 and 655 K in early winter, and at 840, 655, and 465 K in late winter.

Figure 3. Time series of average observed N_20 mixing ratios (ppbv) at the positions of parcels initialized at 840 K, as a function of initial scaled PV (-PV in the SH). Parcels are grouped by initial PV in bins 0.2 x 10-4 s^{-}] wide, centered around the values at the tick marks. Averages are calculated for these ensembles as described in the Fig. 2 caption.

Figure 4. Illustration of gridding procedure. (a) shows predicted N_20 mixing ratios (ppbv) of parcels whose potential temperatures are between 788 and 897 K on day 30 (16 Mar 1993) of the run started 14 Feb 1993; (b) shows the potential temperatures (θ, K) of those parcels; (c) shows the final gridded 840 K N_20 (ppbv) field.

Figure 5. Synoptic maps of N_20 (ppbv) from the trajectory calculations and from observations at 655 K during the two early winter time periods. PV contours in the

region of strong gradients are superimposed on the observed fields. The projection is orthographic, with 0^{o} longitude at the bottom of the plot in the NH and at the top in the SH and 90°E to the right; dashed lines show 30° and 60° latitude circles.

Figure 6. As in Figure 5, but for H_20 (ppmv) for the NH early winter time period.

Figure 7. As in Figure 5, but for N_20 at 840 and 465 K during the two late winter time periods.

Figure 8. Zonal mean N_2O mixing ratios (ppbv) from observations and trajectory calculations as a function of latitude and θ, on day O and 24 of the runs started in Dec 1992, Feb 1993, Aug 1992, and on day O and 20 for the run started in Jun 1992.

Figure 9. Time series of vortex-averaged N_20 mixing ratios (ppmv) as a function of θ in the mid-stratosphere (655 K-- 1300 K) and lower stratosphere (420 K--655 K). Vortex-averages are area weighted, and are computed using the 1.2×10^{-4} s^{-1} scaled PV (-PV in the SH) contour in the lower stratosphere and the 1.4 x 10-4 s1 scaled PV contour in the middle stratosphere as a approximate definition of the vortex edge, Values between 0.02 and 0,025 ppmv are shaded in the middle stratosphere plots, and between 0.16 and 0.18 ppmv in the lower stratosphere plots.

PARCELS STARTED AT 655 K

TRAJECTORIES

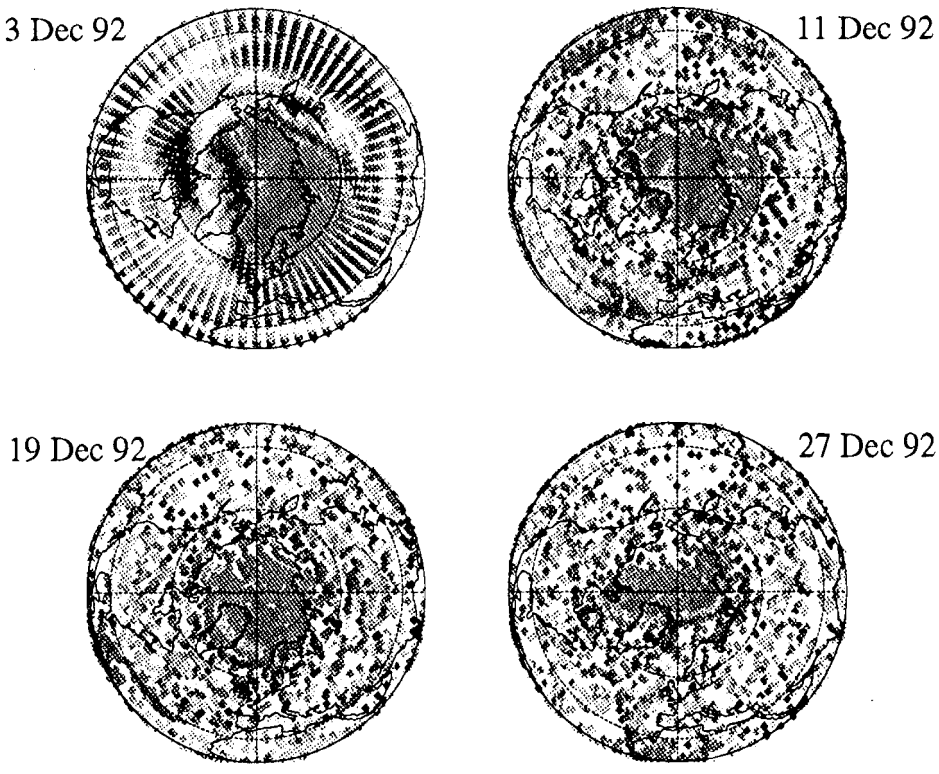

OBSERVATIONS

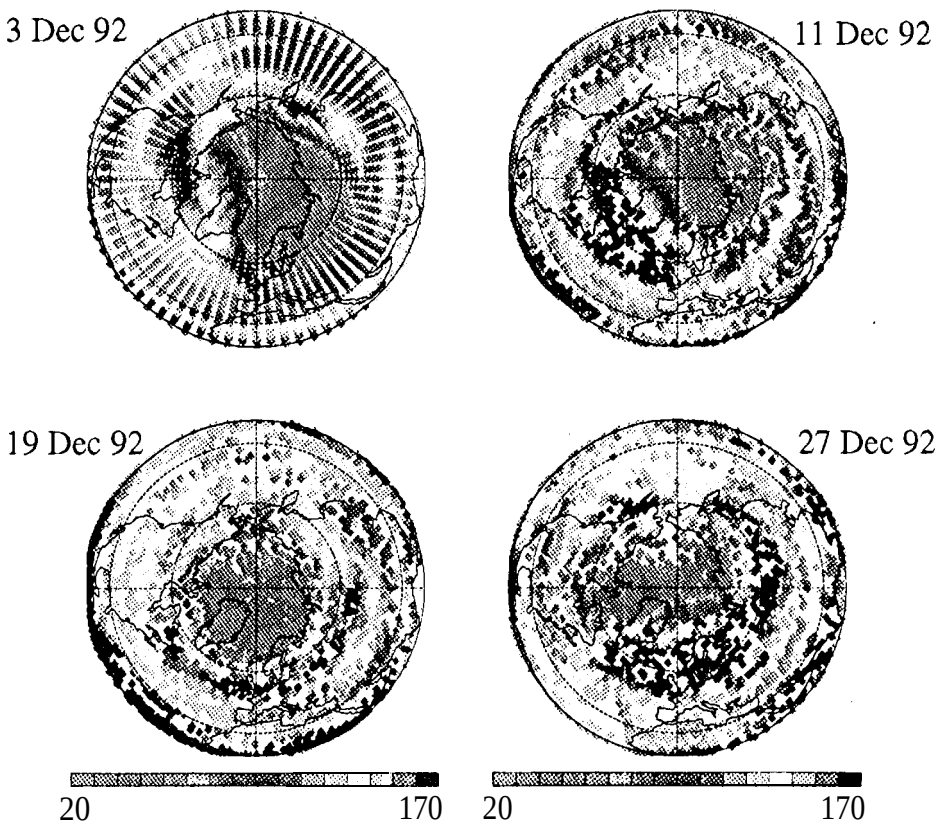

PARCELS STARTED AT 655 K

TRAJECTORIES

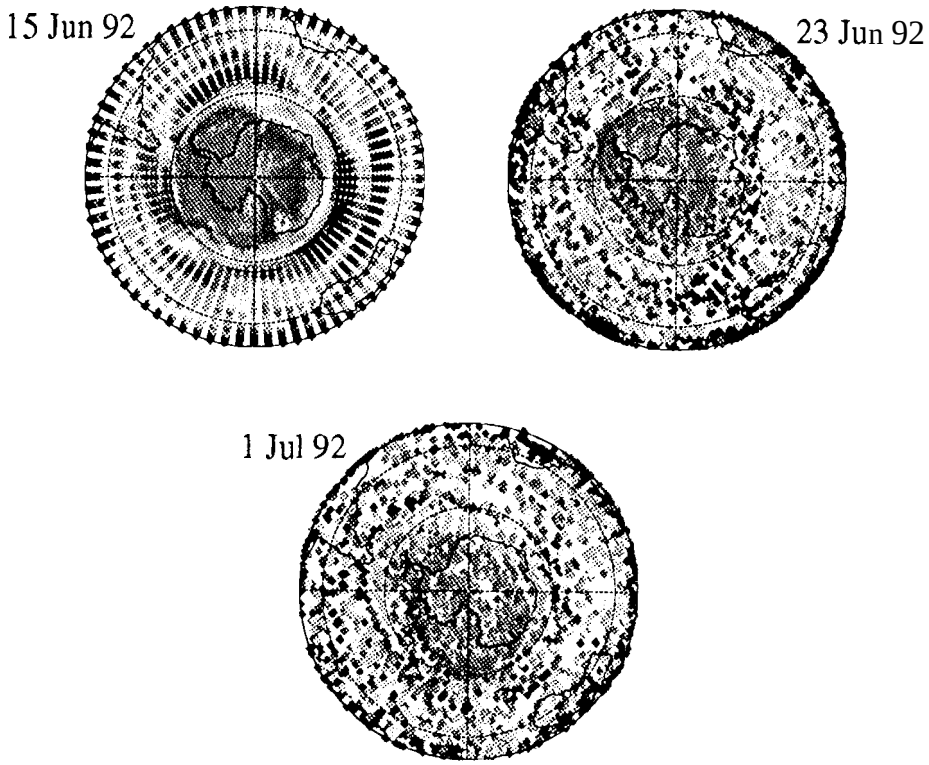

OBSERVATIONS

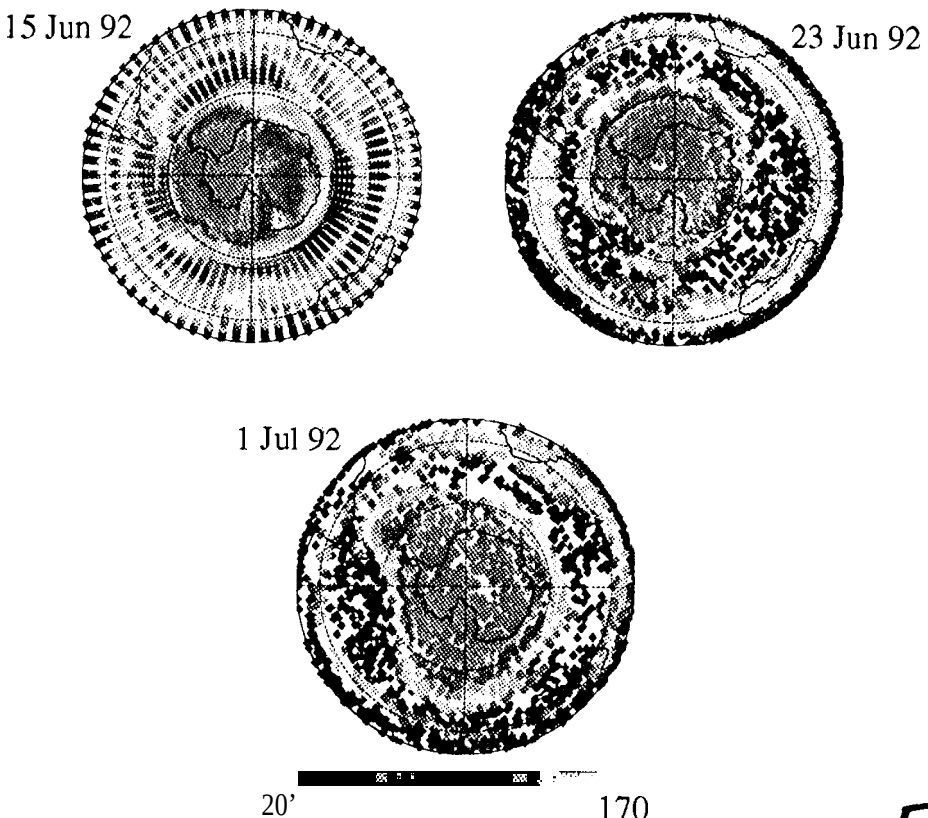

Fig. 16

PARCELS STARTED AT 840 K

TRAJECTORIES

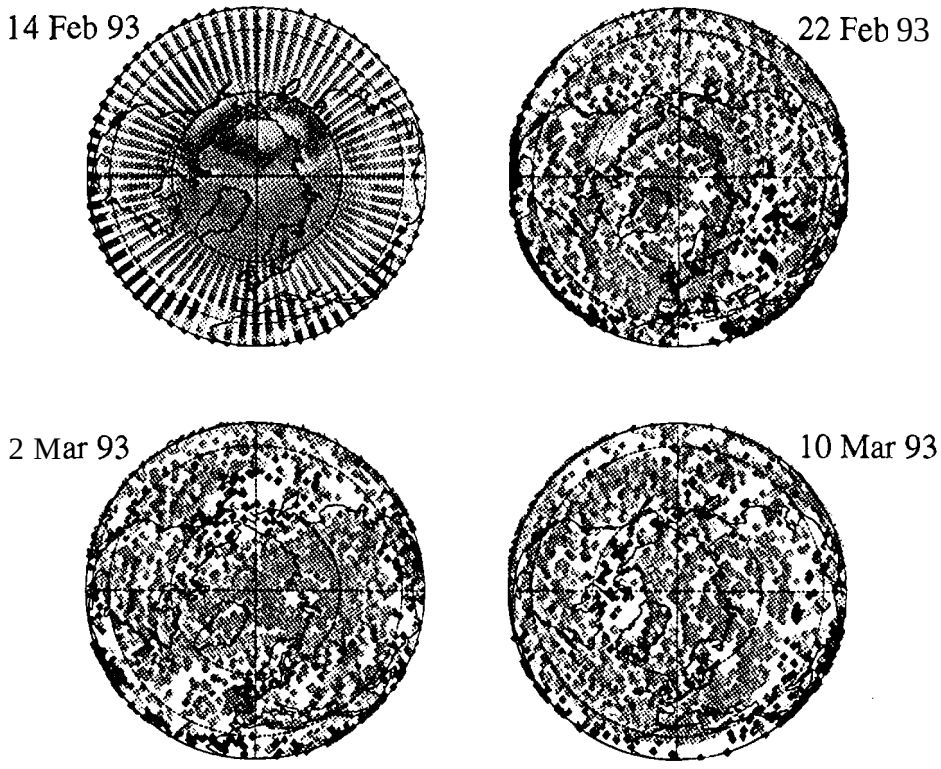

OBSERVATIONS

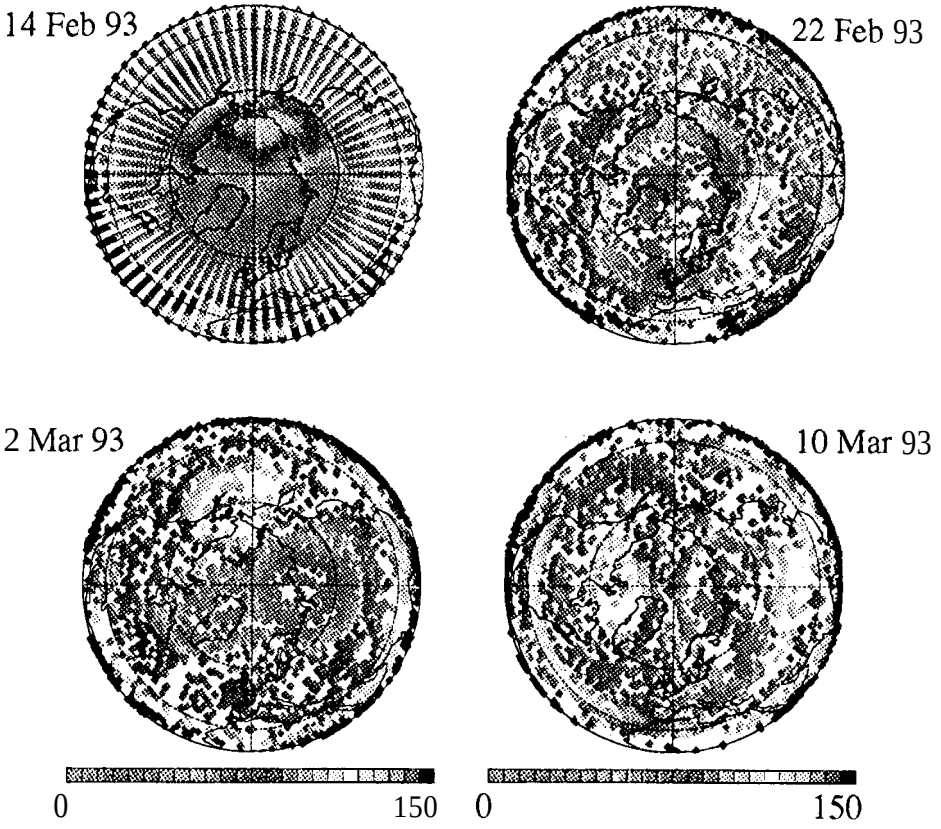

Fig. 1c

PARCELS STARTED AT 655 K

TRAJECTORIES

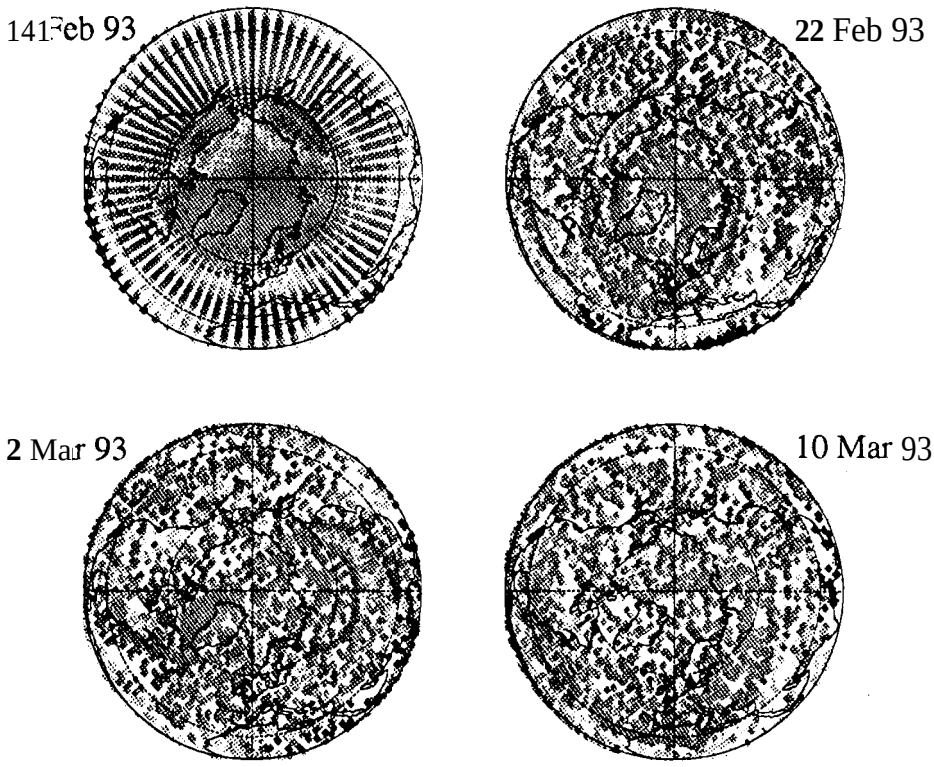

OBSERVATIONS

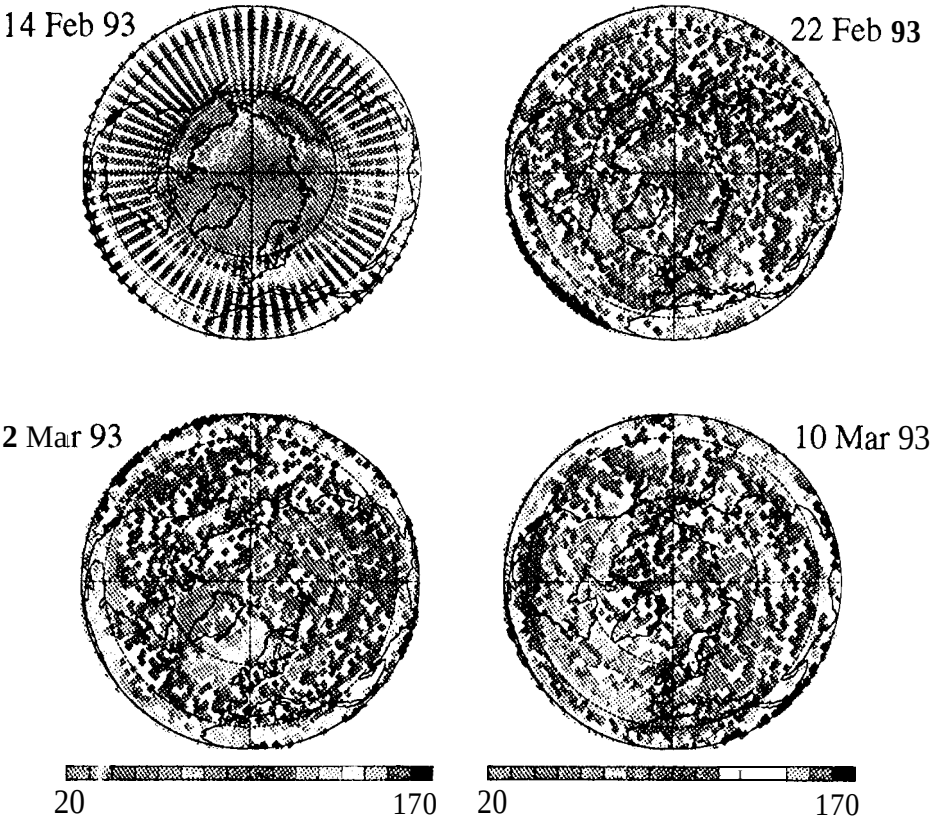

Fig. 1d

PARCELS STARTED AT 465 K

TRAJECTORIES

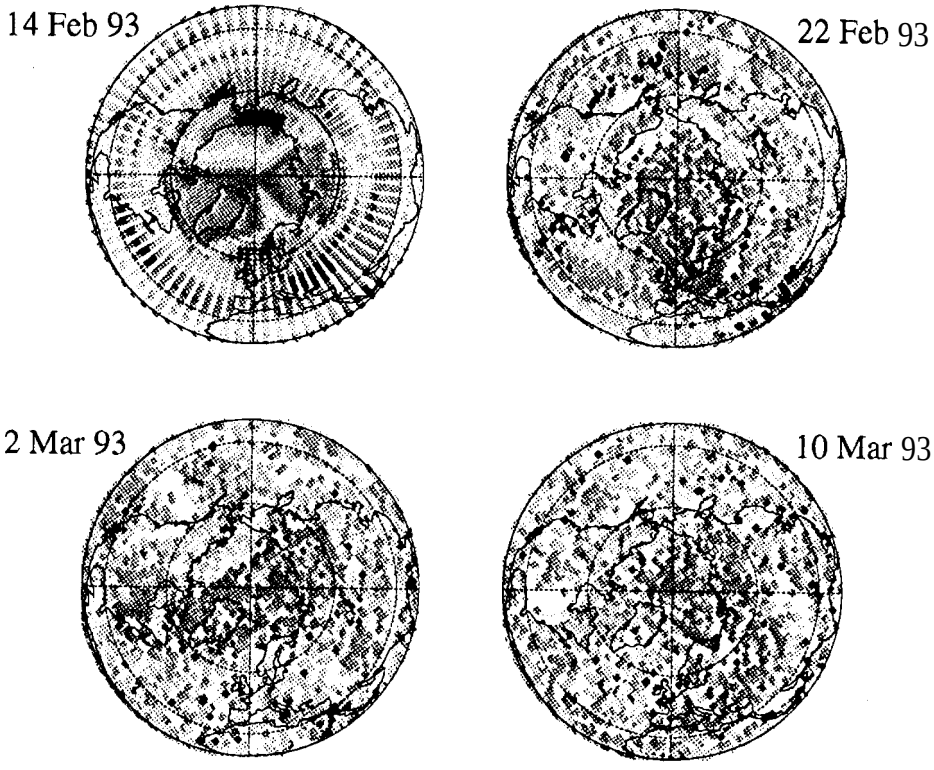

OBSERVATIONS

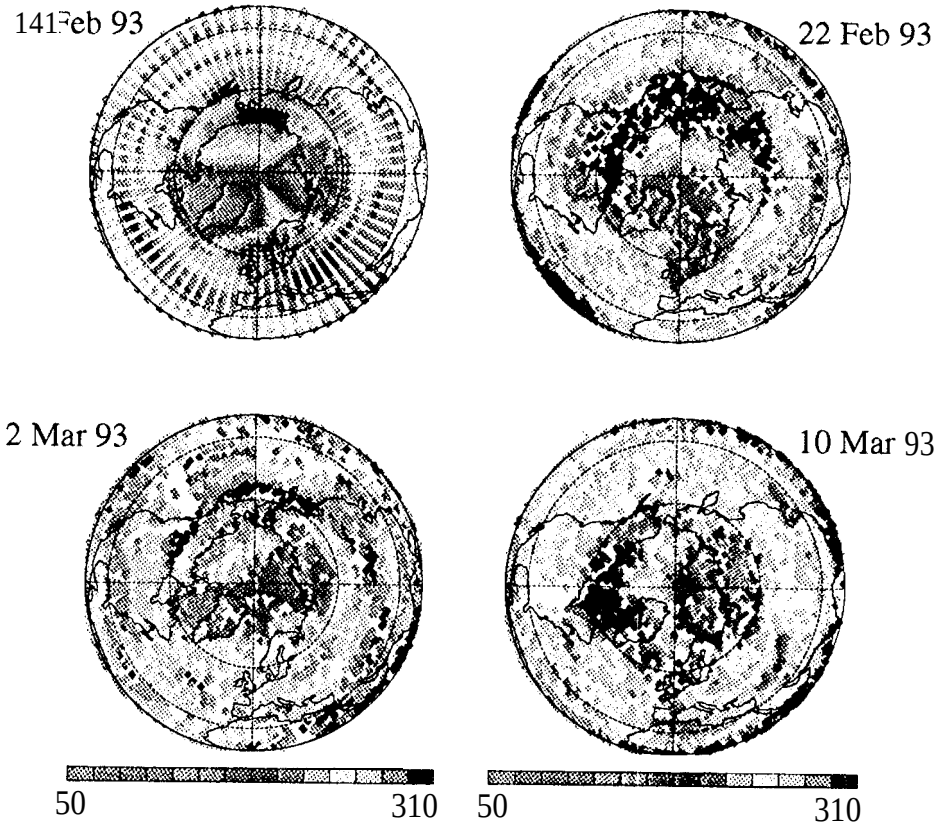

Fig. 1c

PARCELS STARTED AT 840 K

TRAJECTORIES

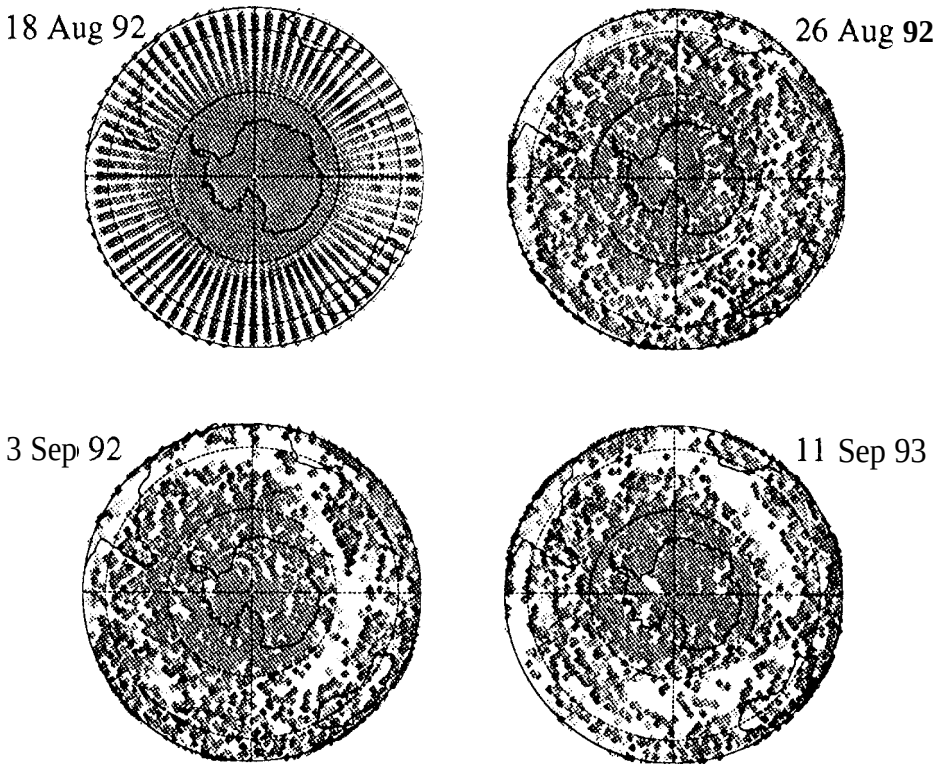

OBSERVATIONS

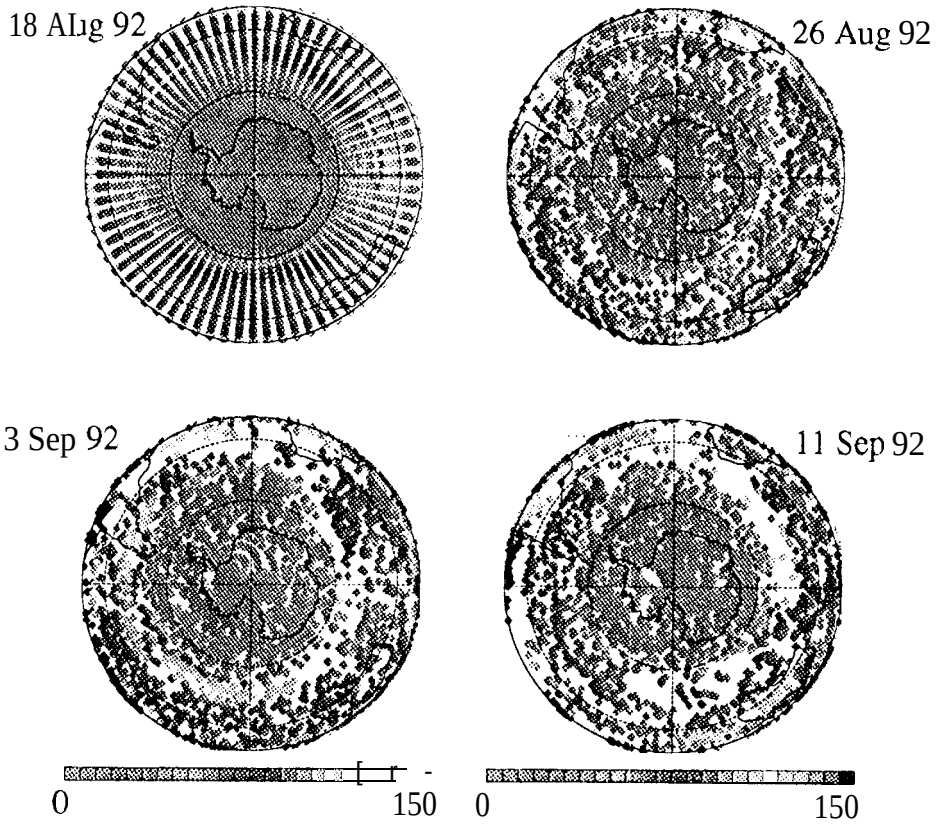

Fig. 1f

PARCELS STARTED AT 655 K

TRAJECTORIES

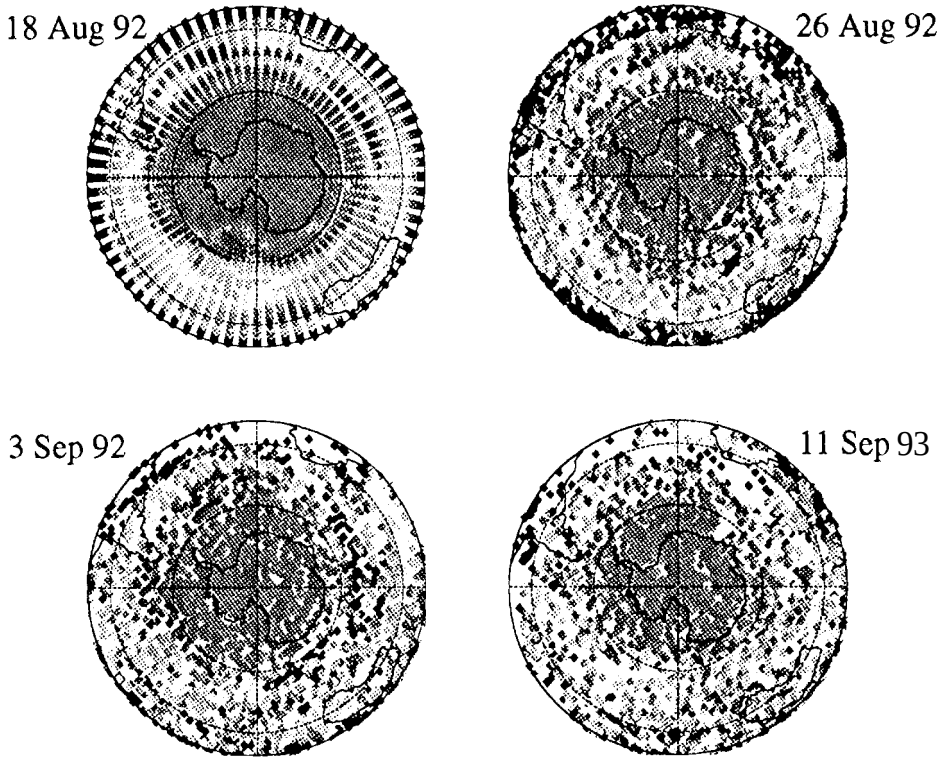

OBSERVATIONS

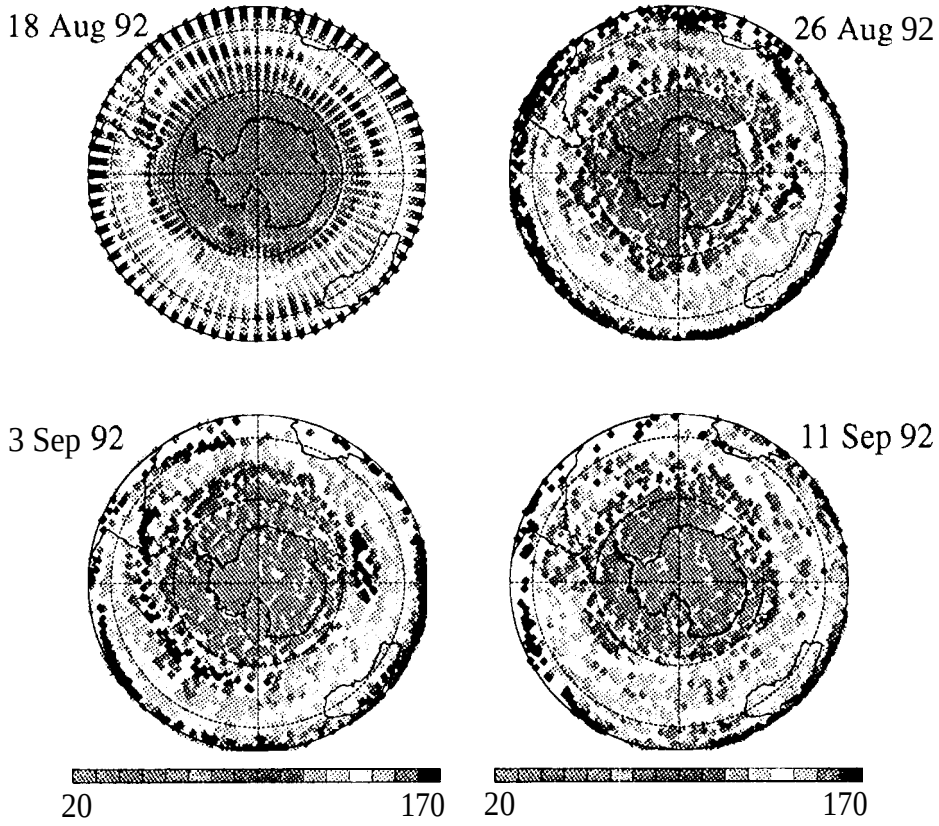

Fig. 1g

PARCELS STARTED AT 465 K

TRAJECTORIES

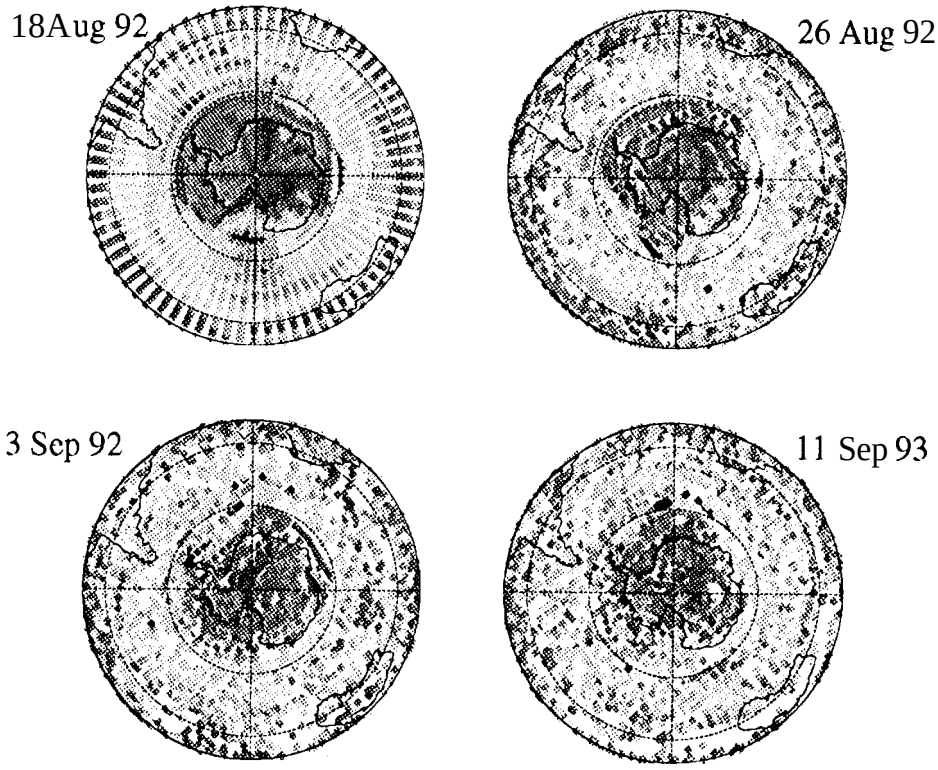

OBSERVATIONS

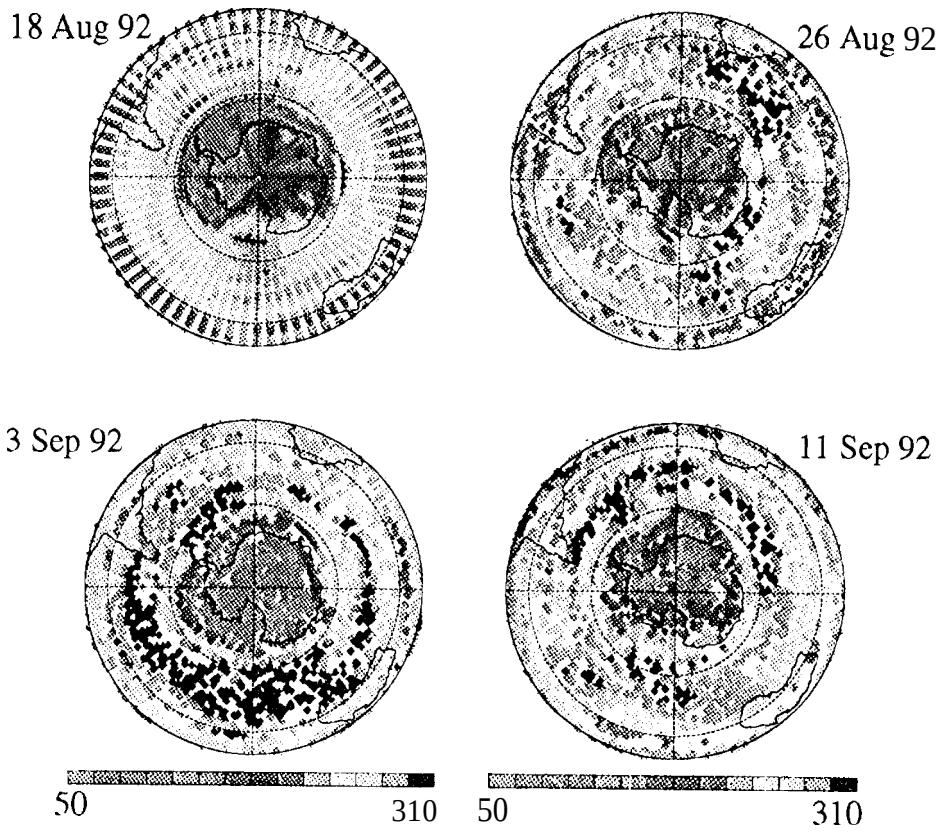

Fig. 1h

PARCELS STARTED AT 840 K

	3Dec92-2Jan93	14 Feb -16 Mar 93	15 Jun - 5 Jul 92	18 Aug -17 Sep 92
N_2O	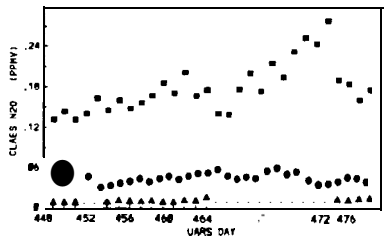	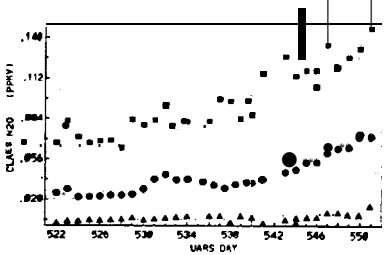	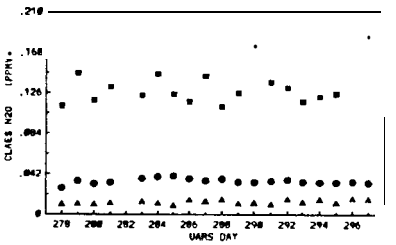	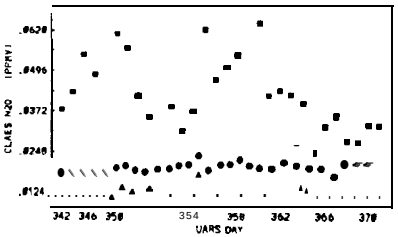
CH_4	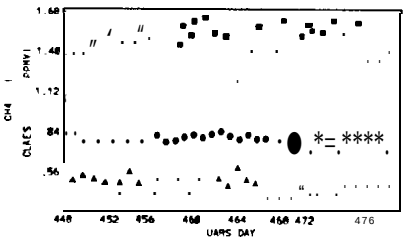	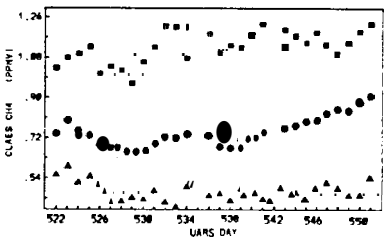	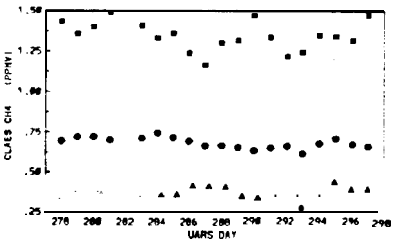	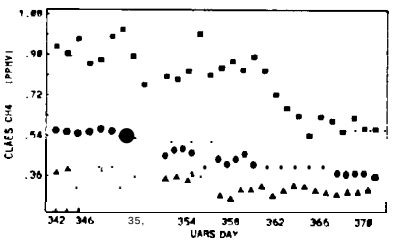
H_2O	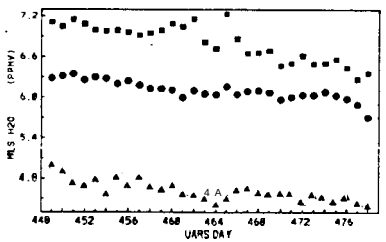	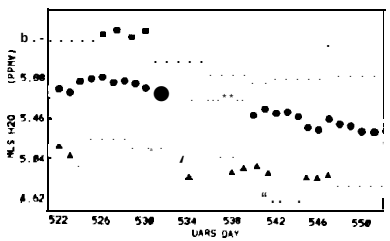		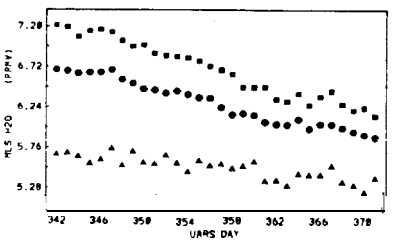

Fig. 2a

PARCELS STARTED AT 655 K

	3Dec92-2Jan93	14 Feb - 16 Mar 93	15 Jun - 5 Jul 92	18 Aug -17 Sep92
N_2O	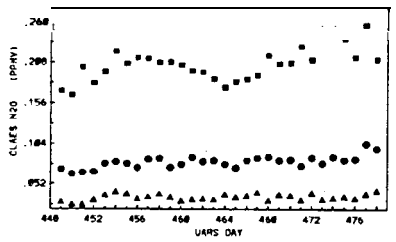	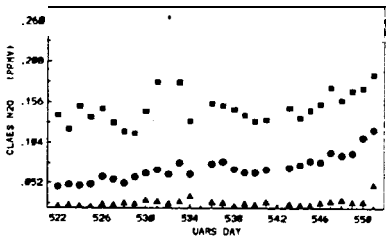	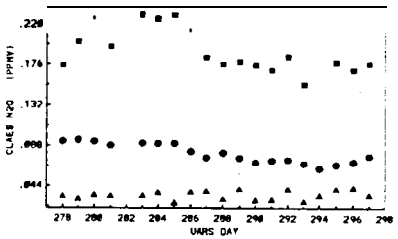	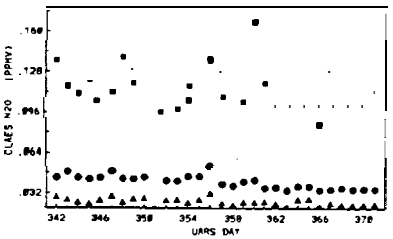
CH_4	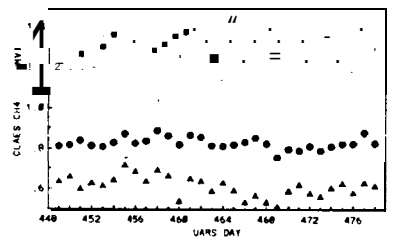	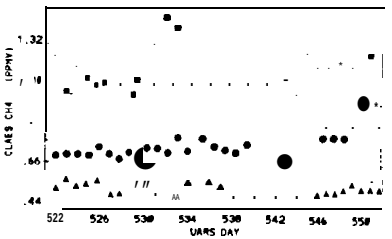	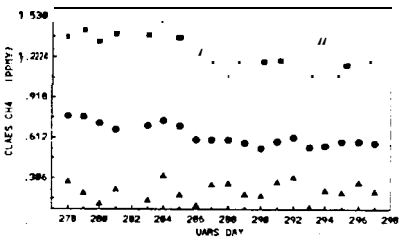	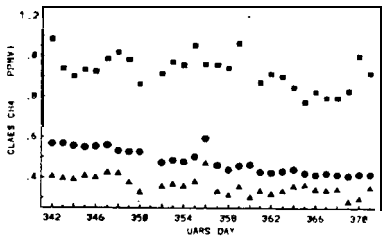
H_2O	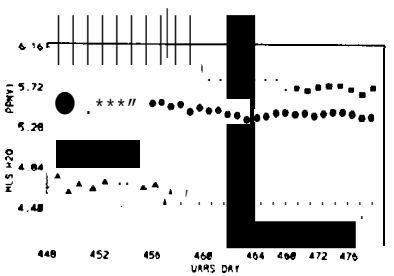	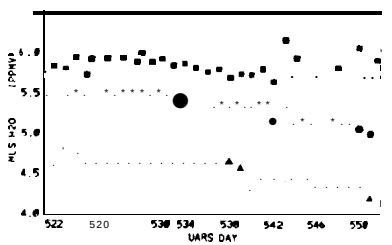		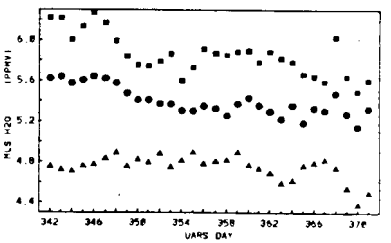

Fig. 26

PARCELS STARTED AT 465 K

14 Feb - 16 Mar 93

18 Aug - 17 Sep 92

N_2O

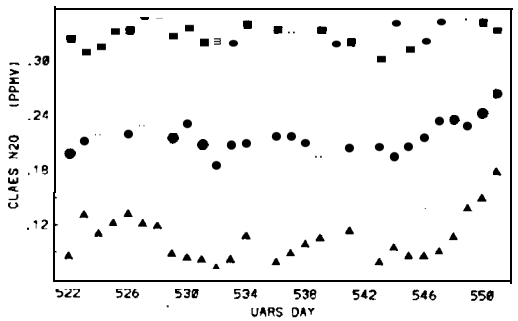

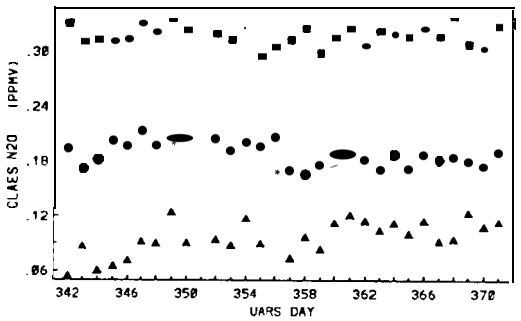

CH_4

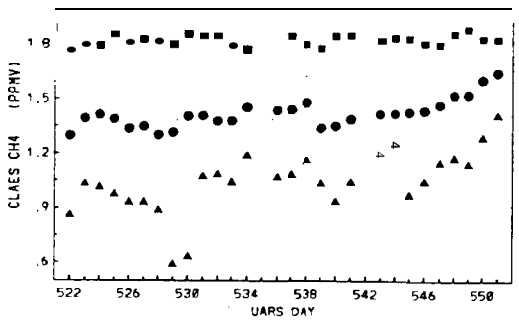

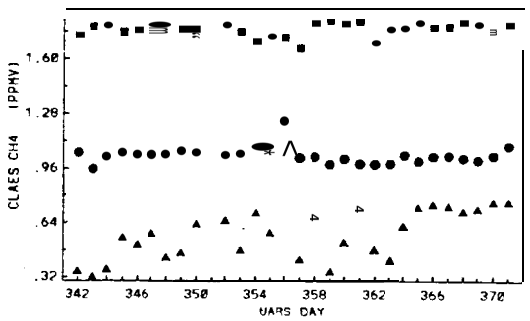

Fig. 2c

PARCELS STARTED AT 840 K

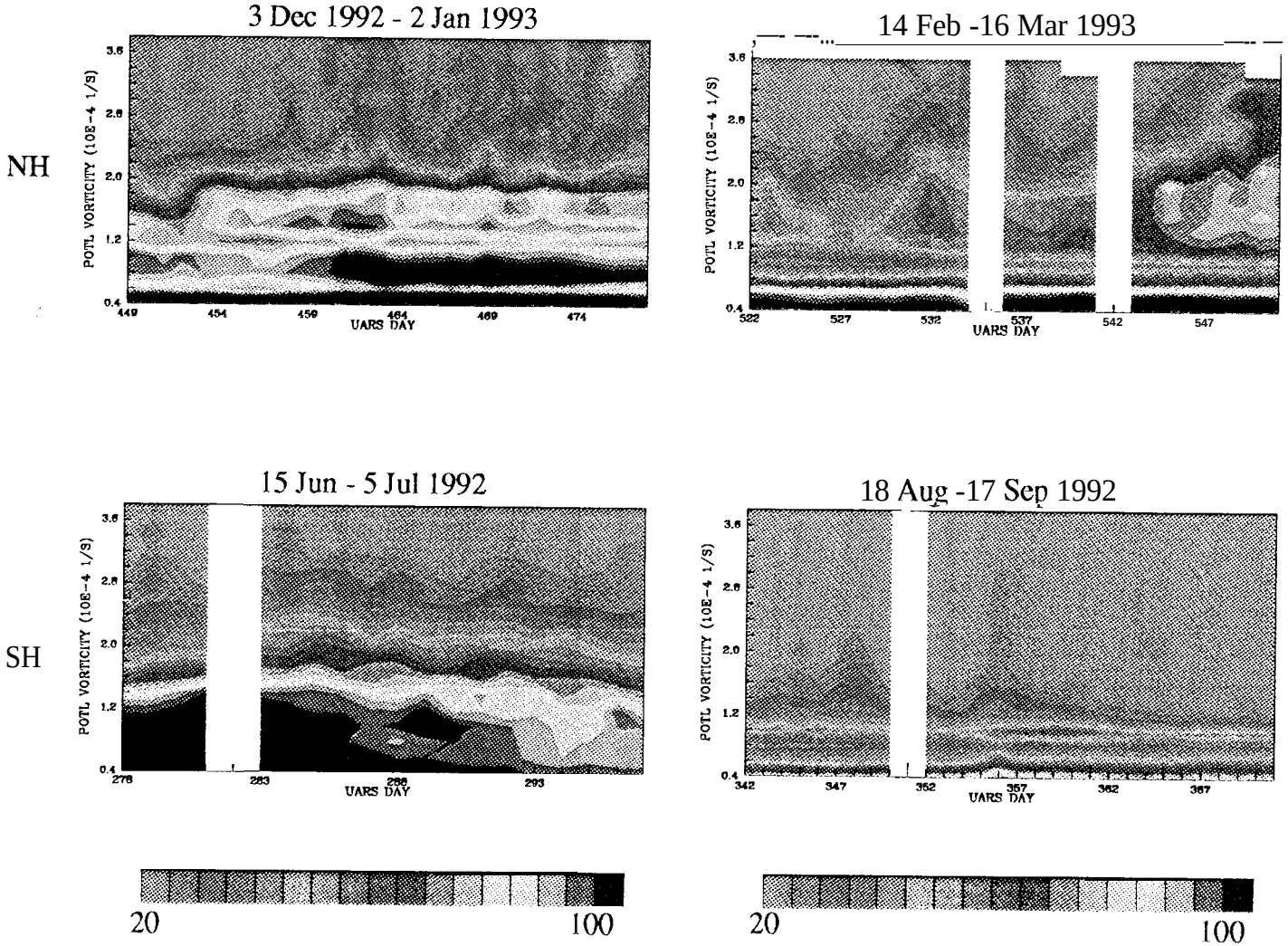

Fig. 3

16 MAR 1993

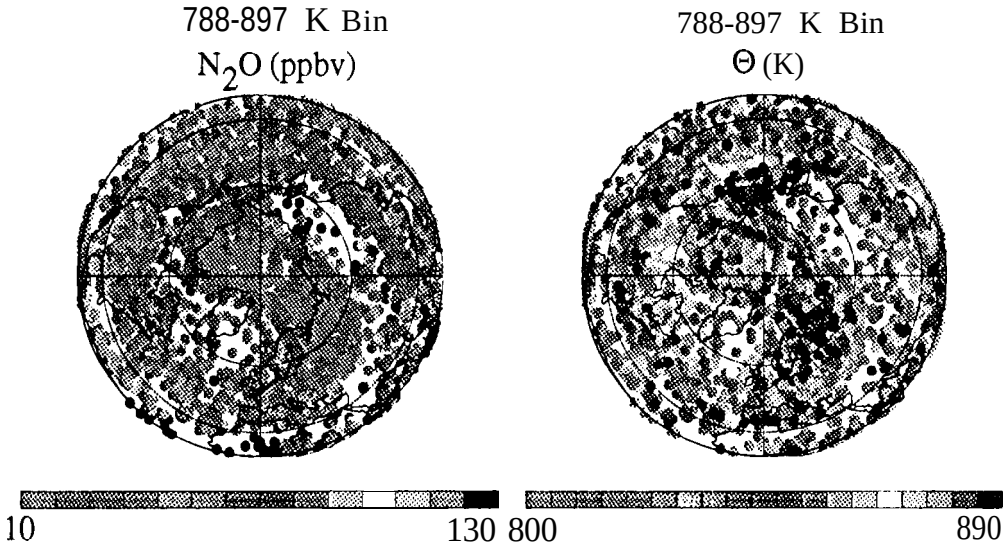

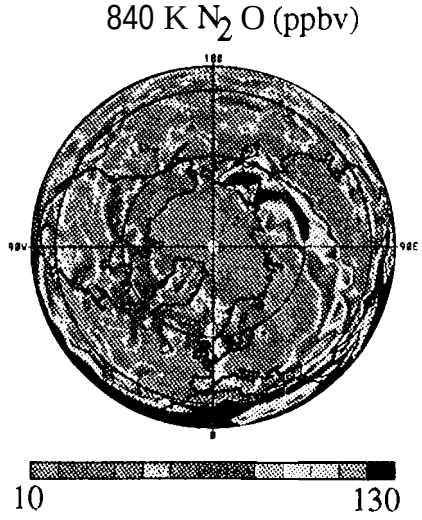

Fig. 4

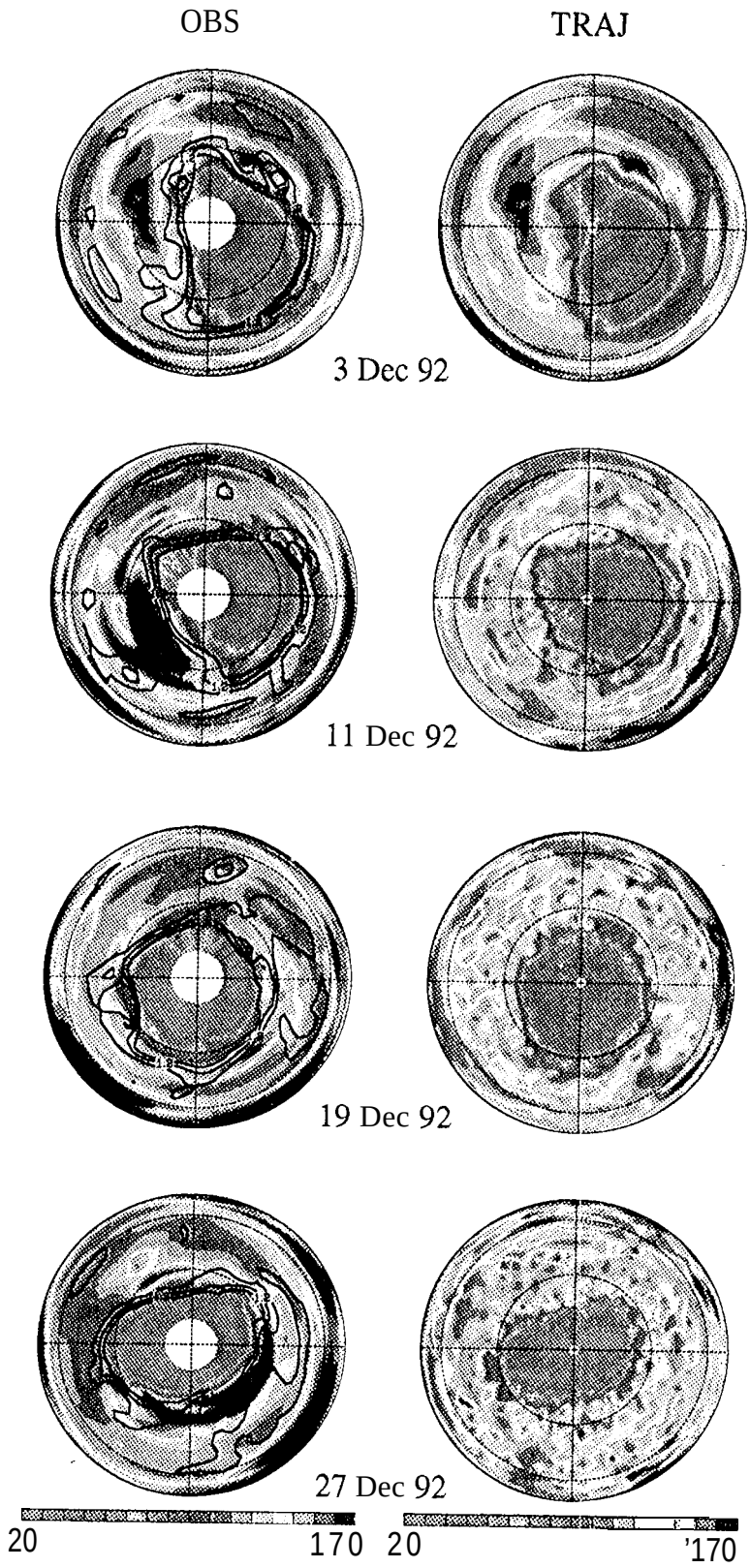
655 K N_2O (ppbv)
OBS
TRAJ
3 Dec 92
11 Dec 92
19 Dec 92
27 Dec 92
20
170
20
'170

Fig. 5a

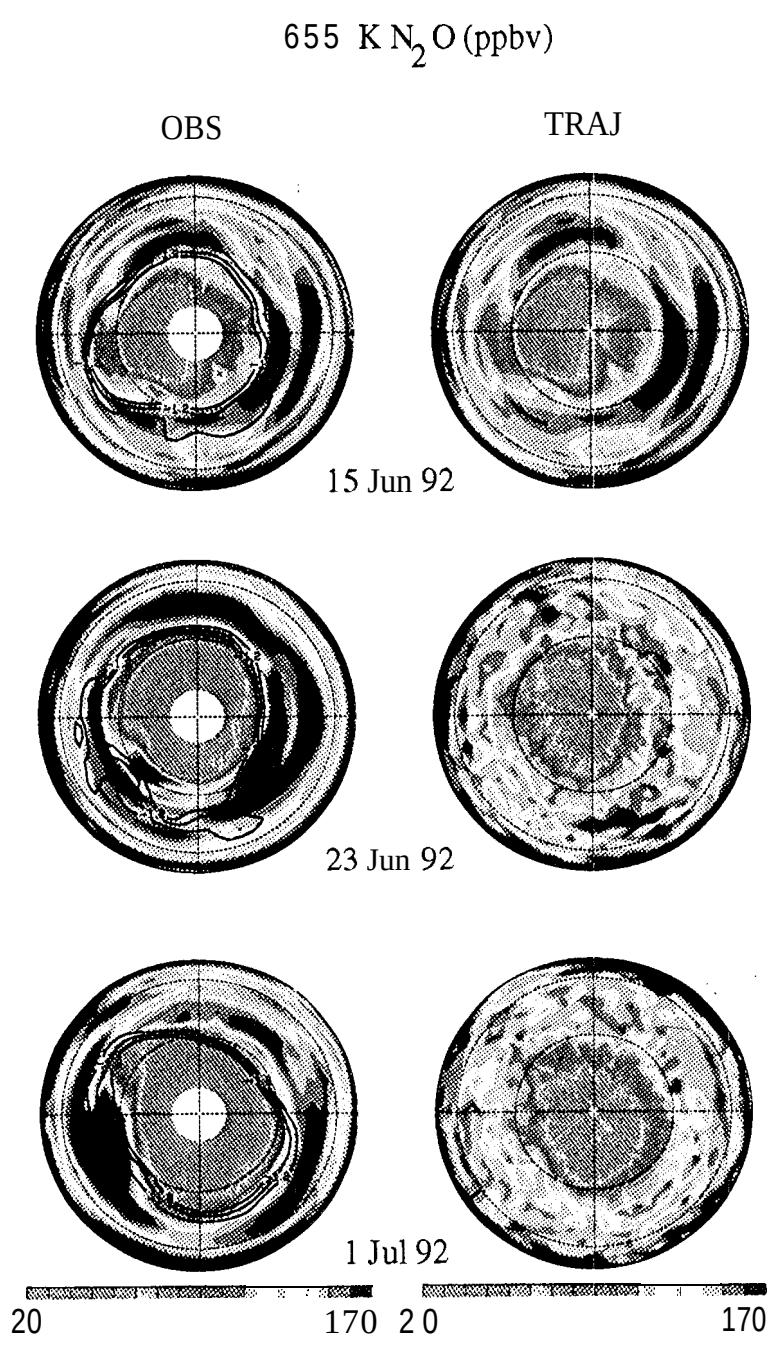

Fig. 5b

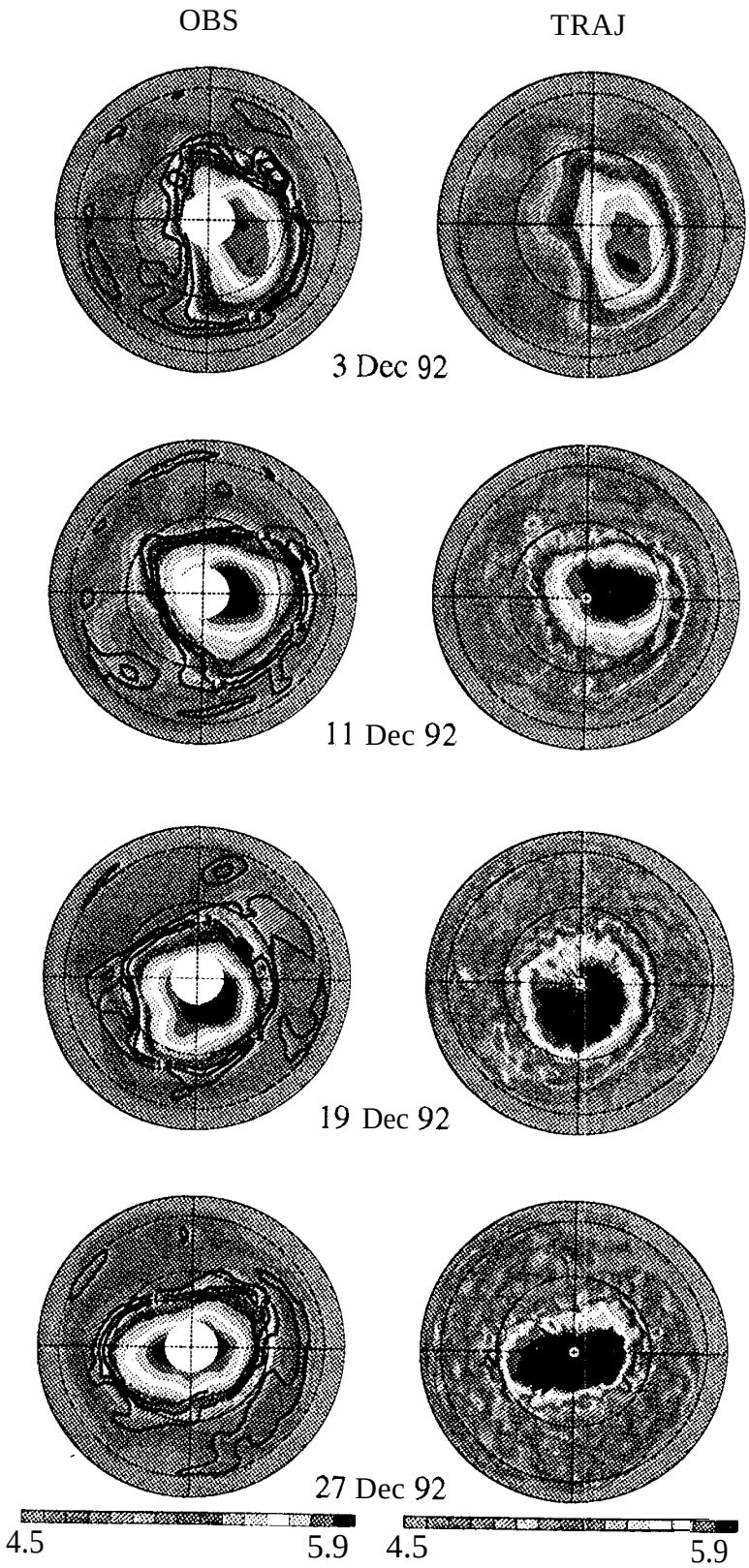
655 K H_2O (ppmv)
OBS
TRAJ
3 Dec 92
11 Dec 92
19 Dec 92
27 Dec 92
4.5
5.9
4.5
5.9

Fig. 6

840 K N_2O (ppbv)

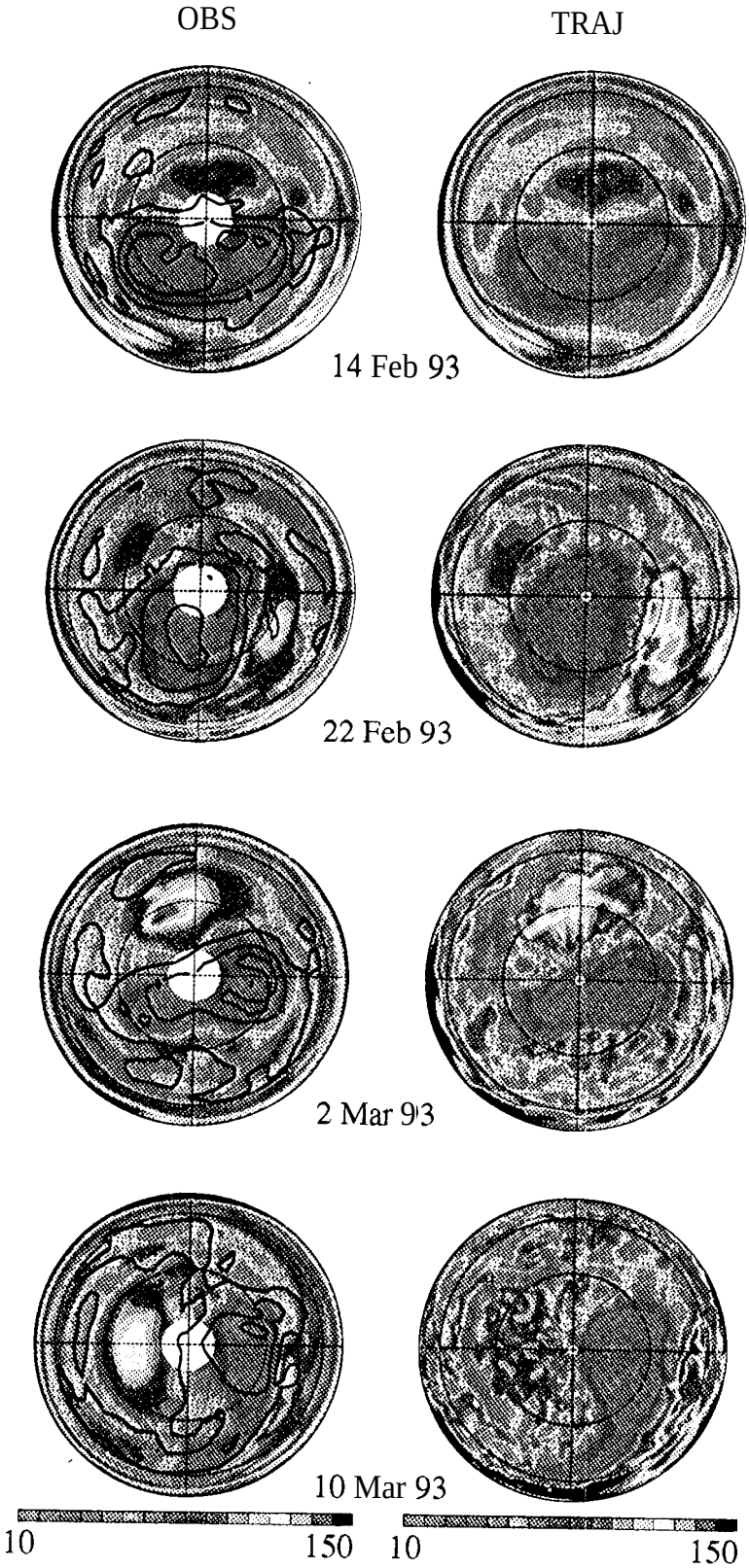

Fig. 7a

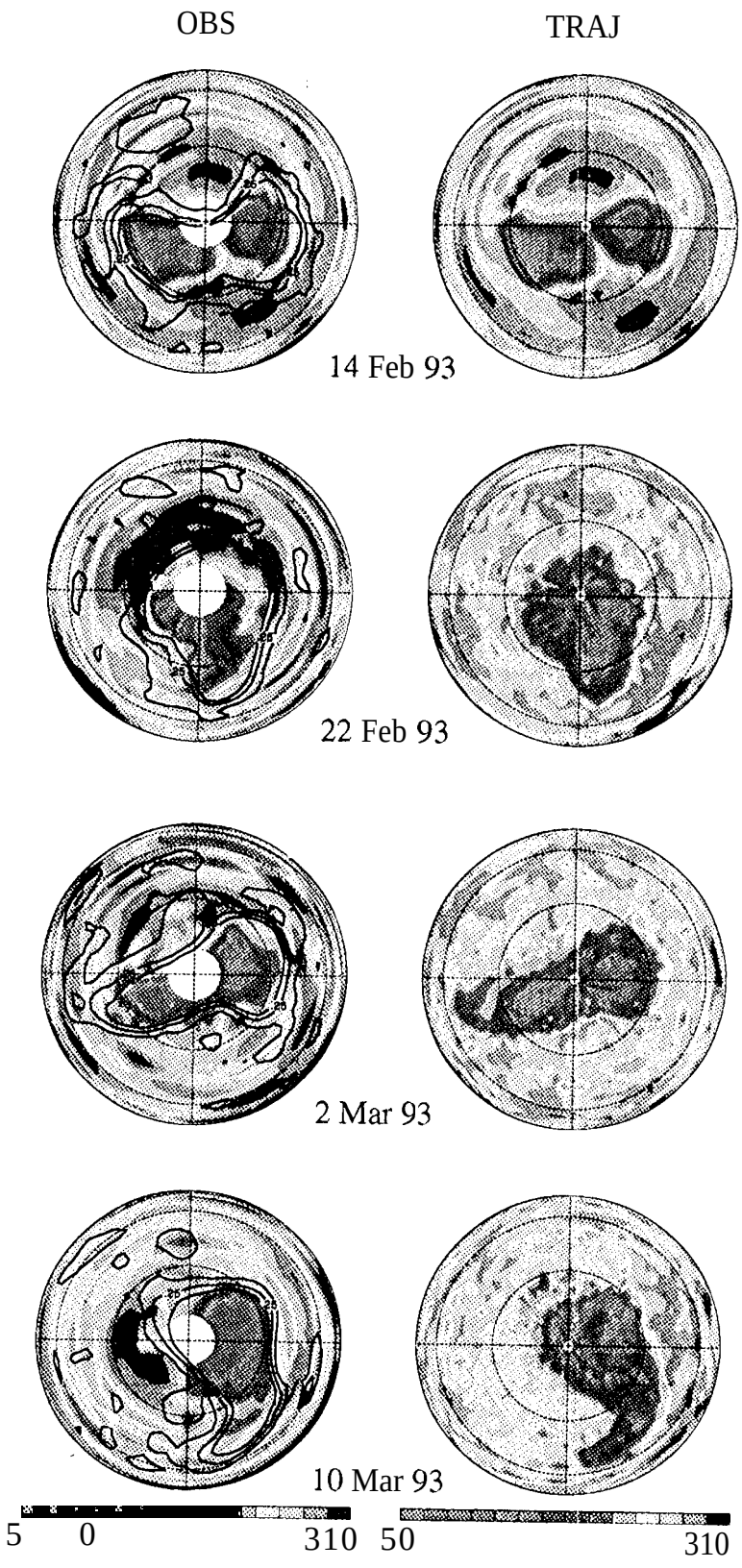
465 K N_2O (ppbv)
OBS
TRAJ
14 Feb 93
22 Feb 93
2 Mar 93
10 Mar 93
5
0
310
50
310

Fig. 7b

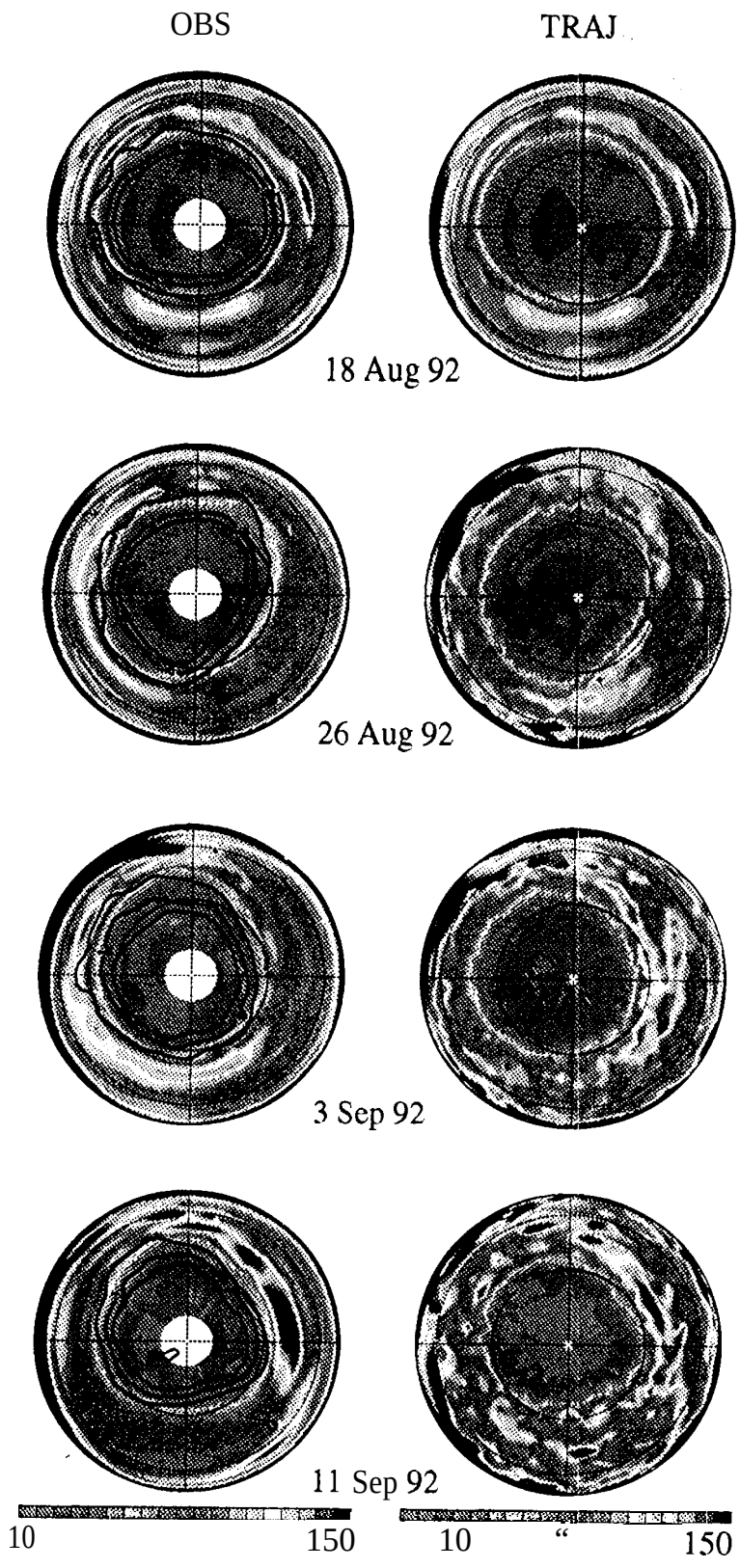
840 K N_2O (ppbv)
OBS
TRAJ
18 Aug 92
26 Aug 92
3 Sep 92
11 Sep 92
10
150
10
150

Fig. 7c

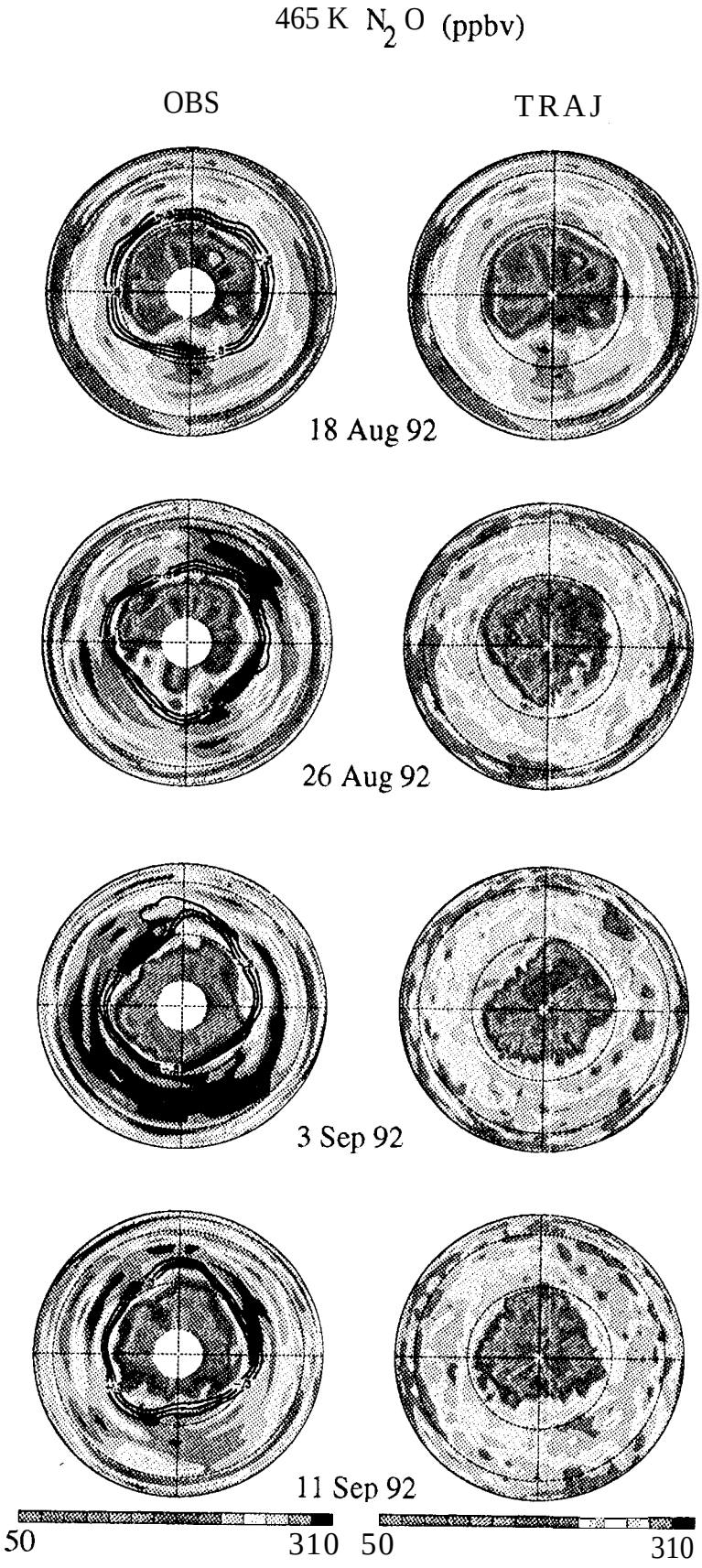
465 K N_2O (ppbv)
OBS
TRAJ
18 Aug 92
26 Aug 92
3 Sep 92
11 Sep 92
50
310
50
310

Fig. 7d

ZONAL MEAN N_2O (ppbv)

OBS TRAJ

3 Dec 1992

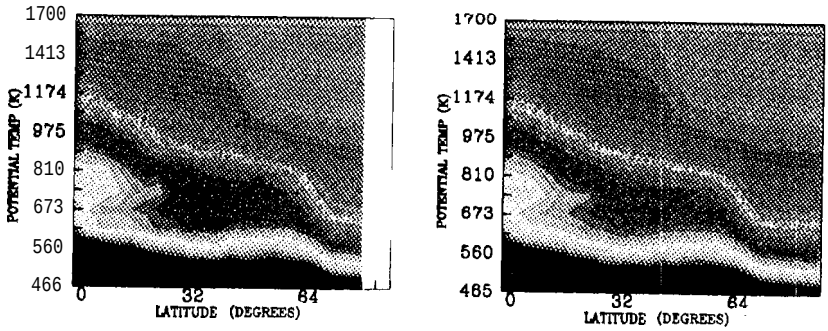

27 Dec 1992

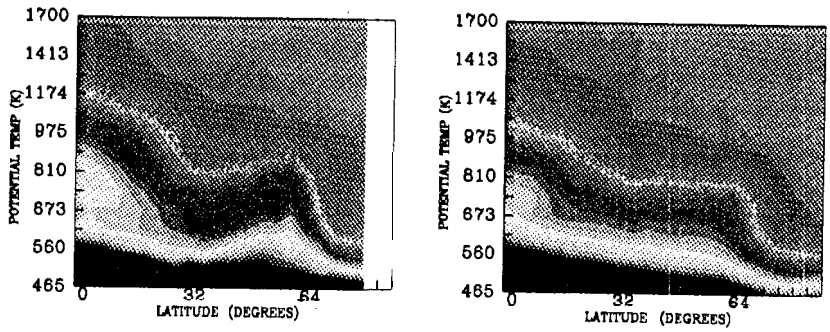

15 Jun 1992

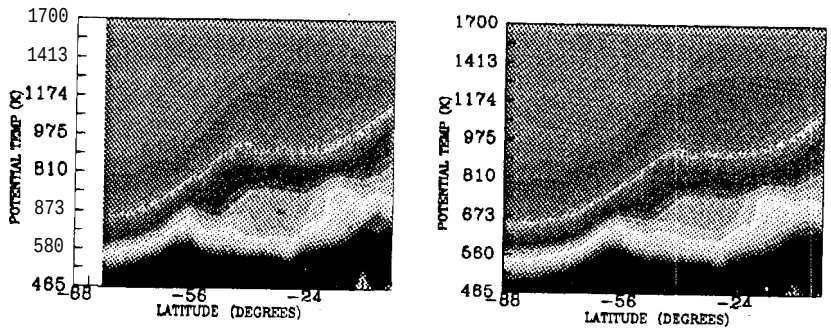

5 Jul 1992

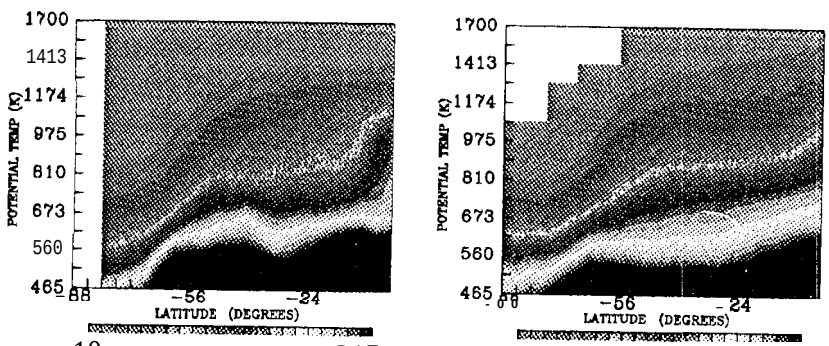

10 215 10 215

Fig. 8a

ZONAL MEAN N_2O (ppbv)

OBS TRAJ

14 Feb 1993

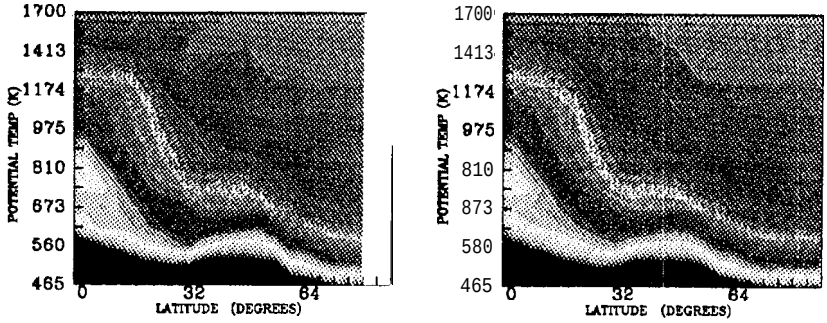

10 Mar 1993

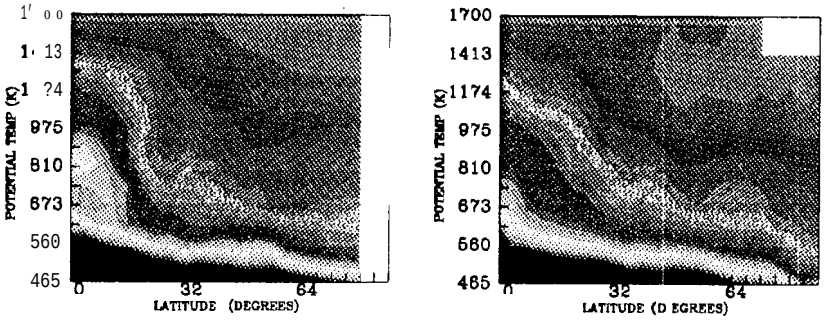

18 Aug 1992

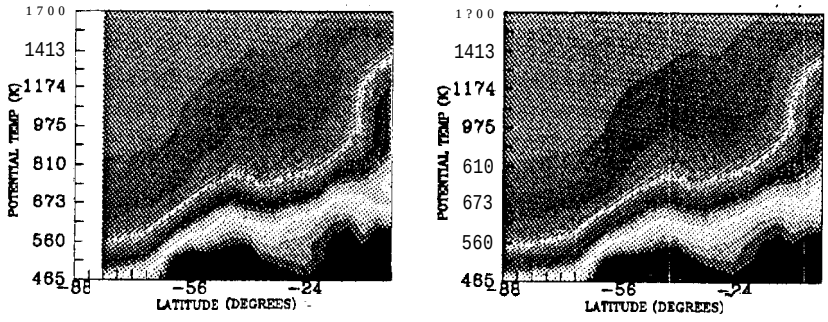

11 Sep 1992

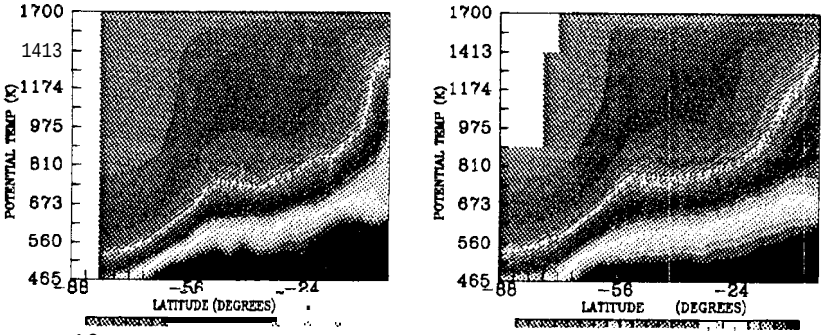

10 215 10 215

Fig. 8b

VORTEX-AVERAGED N_2O (PPMV)

MIDDLE STRATOSPHERE

3 Dec 1992-2 Jan 1993 Obs

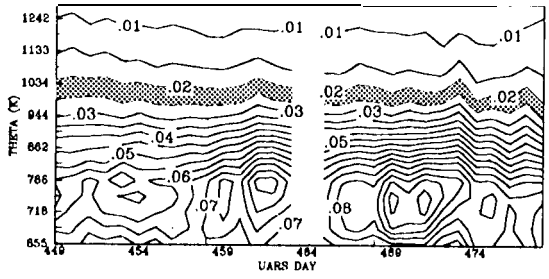

14 Feb - 16 Mar 1993 Obs

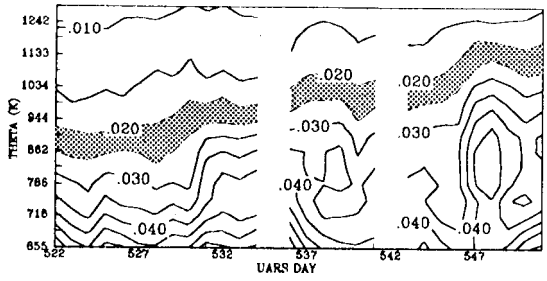

3 Dec 1992 - 2 Jan 1993 Traj

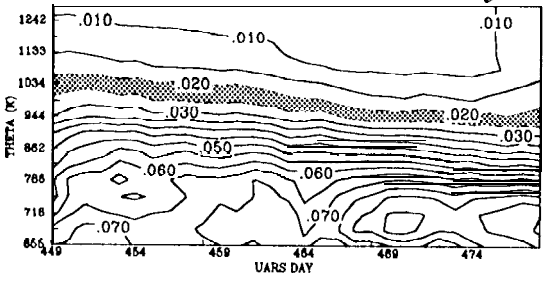

14 Feb - 16 Mar 1993 Traj

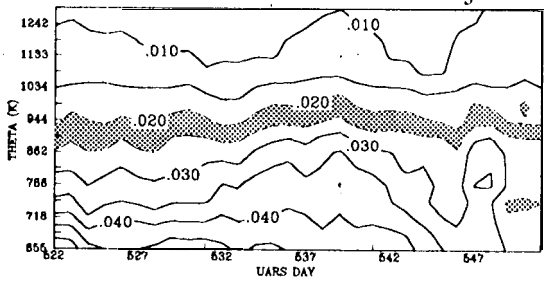

15 Jun - 5 Jul 1992 Obs

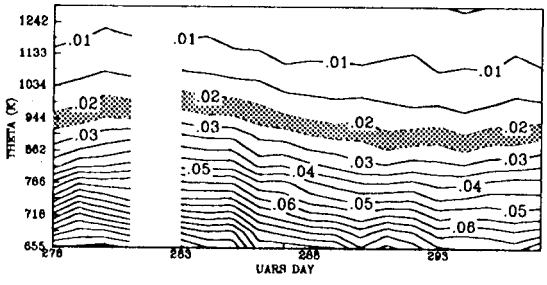

18 Aug - 17 Sep 1992 Obs

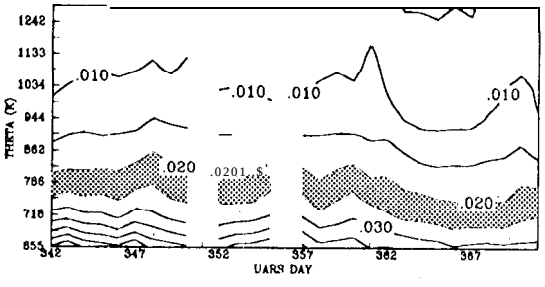

15 Jun -5 Jul 1992 Traj

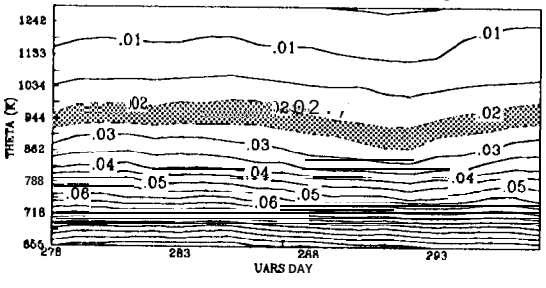

18 Aug - 17 Sep 1992 Traj

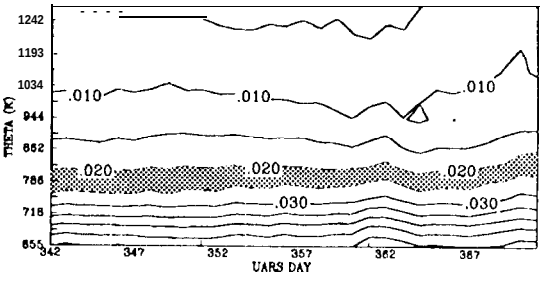

Fig. 9a

VORTEX-AVERAGED N_2O (PPMV)
LOWER STRATOSPHERE

3 Dec 1992 -2 Jan 1993 Obs

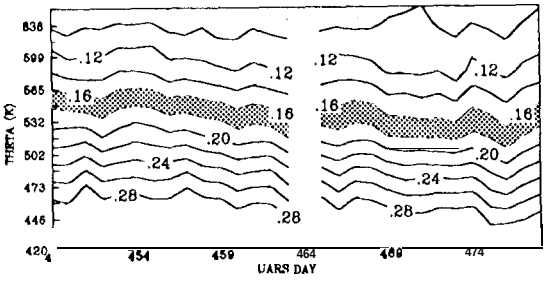

14 Feb - 16 Mar 1993 Obs

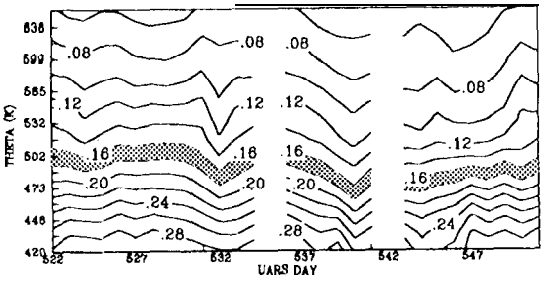

3 Dec 1992 - 2 Jan 1993 Traj

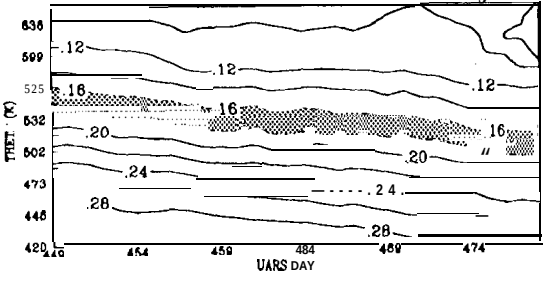

14 Feb -16 Mar 1993 Traj

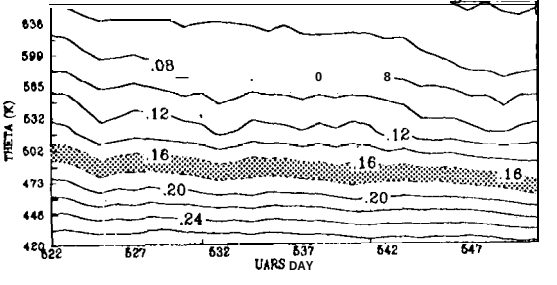

15 Jun - 5 Jul 1992 Obs

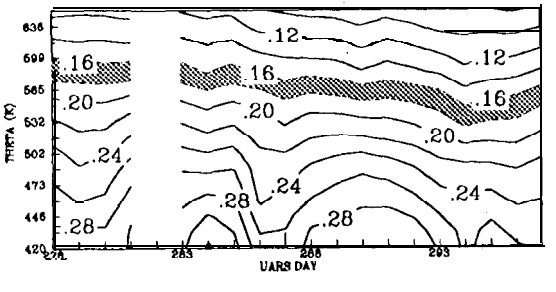

18 Aug - 17 Sep 1992 Obs

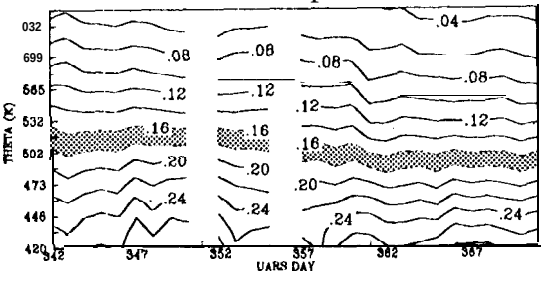

15 Jun - 5 Jul 1992 Traj

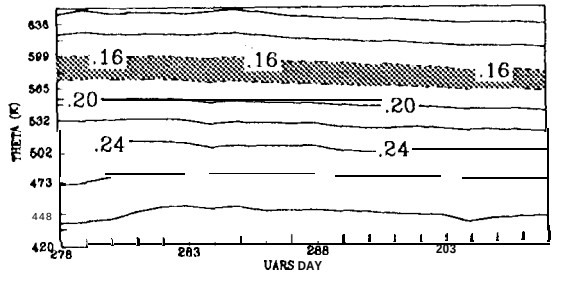

18 Aug -17 Sep 1992 Traj

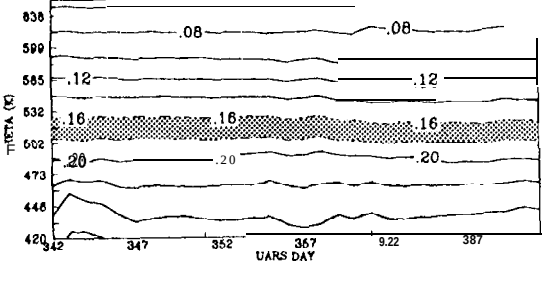

Fig. 9b